

PHOTOCATALYTIC BIREFORMING OF METHANE OVER SILVER-
LANTHANUM MODIFIED GRAPHITIC CARBON NITRIDE WITH TITANIA
NANOCOMPOSITE IN MONOLITH PHOTOREACTOR

BEENISH TAHIR

A thesis submitted in fulfilment of the
requirements for the award of the degree of
Doctor of Philosophy

School of Chemical and Energy Engineering
Faculty of Engineering
Universiti Teknologi Malaysia

APRIL 2019

This thesis is dedicated to my father, who taught me that the best kind of knowledge to have is that which is learned for its own sake. It is also dedicated to my mother, who taught me that even the largest task can be accomplished if it is done one step at a time.

ACKNOWLEDGEMENT

In the name of **Allah Almighty**, the lord of the world, the most Merciful, the most Compassionate who gives me such a power, knowledge and ability to accomplish my goal.

First and foremost, I wish to express my sincere appreciation to my supervisor Prof. Ir. Dr. Nor Aishah Saidina Amin for her encouragement, guidance, critics, friendship and most of all the patience through thick and thin of my study. Without her continued support and interest, this thesis would not have been the same as presented here. I also gratitude to School of Chemical and Energy Engineering (SCEE) Universiti Teknologi Malaysia (UTM) for providing an opportunity to complete this work. I am very thankful to my husband Dr. Muhammad Tahir for his continuous support and motivation, whenever, I was in trouble and despairing.

My fellow postgraduate students at Chemical Reaction Engineering Group (CREG) should also be recognised for their support and encouragement throught the course of this study. My sincere appreciation also extends to all my friends in UTM and others who have provided motivations at various occasions.

Last but not least, I obliged my Mother for her unconditional love and prayers throughout my entire life and particularly through pursuing my doctoral endeavours. I have no words to thank my Father (late) for his motivation and support to achieve this final goal. I am also thankful to my sister Kainat Baqir (Late) and Brothers Jehazaib Baqir and Shahzaib Baqir for their lover for me. I have special love for my sons Muhammad Ibrahim and Muhammad Ahmad who suffered during this period.

ABSTRACT

Photocatalytic conversion of carbon dioxide (CO₂) and methane (CH₄) offers a solution of greenhouse gas mitigation with alternative energy supply. The objective of this study is to design and fabricate photoreactor system and to synthesize silver (Ag) and lanthanum (La) modified protonated carbon nitride (pCN) coupled titanium dioxide (TiO₂) photocatalysts for enhanced photocatalytic CO₂ reduction with CH₄ in the presence of water to fuels. The ternary Ag-La/pCN-TiO₂ composite catalysts were synthesized through sonicated assisted hydrothermal and sol-gel methods. The performance of nanomaterials was investigated using photocatalytic reforming of methane (BRM), dry reforming of methane (DRM), steam reforming of methane and steam reforming of carbon dioxide in a fixed-bed and monolith photoreactors under UV and visible light irradiations. Ag/La-loaded protonated carbon nitride nanotubes (pCNNT) produced both carbon monoxide (486 μmol g-cat⁻¹ h⁻¹) and hydrogen (79 μmol g-cat⁻¹ h⁻¹) under visible light irradiations, while productivity was highest in BRM process, which was further improved in a monolith photoreactor with CO and H₂ production rate of 770 and 891 μmol g-cat⁻¹ h⁻¹, respectively. Furthermore, using pCN-TiO₂ composite loaded with La, higher amount of CO was obtained, while production of H₂ had increased with Ag-loading. More importantly, a remarkable improvement in productivity of both CO and H₂ with H₂/CO ratio greater than one was obtained using Ag-La co-loaded pCN-TiO₂ composite catalyst. The highest CO and H₂ production rate of 2105 and 2387 μmol g-cat⁻¹ h⁻¹, respectively, were obtained using BRM process in a monolith photoreactor. The performance of monolith photoreactor was 1.4 and 3.2 fold higher for CO and H₂ rich synthesis gas (syngas) production than using fixed-bed reactor over the composite catalyst under UV-light irradiations. The reaction mechanism based on Z-scheme system for DRM and BRM was successfully developed under UV light irradiation, while direct electron transfer was observed under visible light irradiations. The quantum efficiency of 4.07 % and 4.624 % was achieved for CO and H₂ production, respectively in a monolith photoreactor, while it was only 1.144 % and 0.548 % in a fixed-bed photoreactor during BRM under UV-light irradiations. Among the operating parameters, feed ratio was the influential parameter to maximize yield and selectivity. The stability test revealed prolonged life and reusability of Ag-La/pCN-TiO₂ composite photocatalyst in three cyclic runs. The Langmuir-Hinshelwood model confirms surface reactions due to efficient sorption process in a monolith photoreactor over composite catalysts. In conclusion, Ag-La loaded pCN-TiO₂ composite catalyst and monolith photoreactor via BRM provided an ideal system to get hydrogen enrich syngas production for renewable fuels productions.

ABSTRAK

Penukaran fotobermangkin karbon dioksida (CO_2) dan metana (CH_4) menawarkan penyelesaian pengurangan gas rumah hijau dengan bekal tenaga alternatif. Objektif kajian ini adalah untuk merekabentuk dan menghasilkan sistem fotoreaktor dan untuk mensintesis fotomangkin karbon nitrida berproton (pCN) gandingan titanium dioksida (TiO_2) terubahsuai dengan perak (Ag) dan lantanum (La) untuk meningkatkan penurunan CO_2 fotobermangkin dengan CH_4 dalam kehadiran air kepada bahan api. Pemangkin komposit ketiga Ag-La/pCN- TiO_2 disintesis melalui kaedah hidrotermal dan sol-gel dibantu dengan sonikasi. Prestasi nanobahan dikaji dengan menggunakan dwipengubahan fotomangkin metana (BRM), pengubahan kering metana (DRM), pengubahan wap metana dan pengubahan wap karbon dioksida dalam fotoreaktor lapisan tetap dan monolit di bawah penyinaran cahaya UV dan nampak. Nanotub karbon nitrida berproton termuat Ag/La (pCNNT) menghasilkan kedua-dua karbon monoksida ($486 \mu\text{mol g-cat}^{-1} \text{h}^{-1}$) dan hidrogen ($79 \mu\text{mol g-cat}^{-1} \text{h}^{-1}$) di bawah penyinaran cahaya nampak, sementara produktiviti tertinggi dalam proses BRM, yang bertambah baik dalam fotoreaktor monolit dengan kadar penghasilan CO dan H_2 masing-masing sebanyak 770 dan $891 \mu\text{mol g-cat}^{-1} \text{h}^{-1}$. Selain itu, dengan menggunakan komposit pCN- TiO_2 termuat dengan La, jumlah CO yang lebih tinggi diperolehi, manakala penghasilan H_2 meningkat dengan pemuatan Ag. Lebih penting lagi, peningkatan produktiviti kedua-dua CO dan H_2 dengan nisbah H_2/CO lebih besar daripada satu diperolehi dengan menggunakan pemangkin komposit pCN- TiO_2 yang dimuatkan bersama Ag-La. Kadar penghasilan CO dan H_2 tertinggi masing-masing sebanyak 2105 dan $2387 \mu\text{mol g-cat}^{-1} \text{h}^{-1}$ diperolehi dengan menggunakan proses BRM dalam fotoreaktor monolit. Prestasi fotoreaktor monolit adalah 1.4 dan 3.2 kali ganda lebih tinggi bagi penghasilan gas sintesis yang kaya dengan CO dan H_2 (singas) berbanding dengan menggunakan reaktor lapisan tetap terhadap mangkin komposit di bawah penyinaran cahaya UV. Mekanisme tindak balas berasaskan sistem skema Z untuk DRM dan BRM berjaya dibangunkan di bawah penyinaran cahaya UV, manakala pemindahan elektron langsung diperhatikan di bawah penyinaran cahaya nampak. Kecekapan kuantum 4.07% dan 4.624% dicapai untuk pengeluaran CO dan H_2 , masing-masing di dalam fotoreaktor monolit, manakala hanya 1.144% dan 0.548% di dalam fotoreaktor lapisan tetap semasa BRM di bawah penyinaran cahaya UV. Antara parameter operasi, nisbah suapan adalah parameter berpengaruh untuk memaksimumkan hasil dan kepemilihan. Ujian kestabilan menunjukkan hayat berpanjangan dan kebolehgunaan semula fotomangkin komposit Ag-La/pCN- TiO_2 dalam tiga kitaran larian. Model Langmuir-Hinshelwood mengesahkan tindak balas permukaan disebabkan oleh proses penyerapan yang cekap di dalam fotoreaktor monolit melalui mangkin komposit. Kesimpulannya, mangkin komposit pCN- TiO_2 yang dimuatkan Ag-La dan fotoreaktor monolit melalui BRM menyediakan sistem yang ideal untuk mendapatkan singas diperkaya hidrogen untuk penghasilan bahan api yang boleh diperbaharu.

TABLE OF CONTENTS

	TITLE	PAGE
	DECLARATION	ii
	DEDICATION	iii
	ACKNOWLEDGEMENT	iv
	ABSTRACT	v
	ABSTRAK	vi
	TABLE OF CONTENTS	vii
	LIST OF TABLES	xv
	LIST OF FIGURES	xvii
	LIST OF ABBREVIATIONS	xxvi
	LIST OF SYMBOLS	xxvii
	LIST OF APPENDICES	xxviii
CHAPTER 1	INTRODUCTION	1
1.1	Background Overview	1
1.2	Photocatalytic CO ₂ Reforming of CH ₄	2
1.3	Problem Statement	7
1.4	Research Hypothesis	8
1.5	Research Objectives	10
1.6	Research Scope	10
1.7	Research Significance	12
1.8	Layout of Thesis	13
CHAPTER 2	LITERATURE REVIEW	14
2.1	Technologies for Conversion of Greenhouse Gases	14
2.2	Photocatalytic CO ₂ Reforming of CH ₄	17
2.2.1	Fundamentals in Catalytic and Photocatalytic Process	17
2.2.2	Photocatalysis Steps in CO ₂ Reduction with CH ₄	18

2.2.3	Reaction Pathways in Photocatalytic CO ₂ Reduction with CH ₄	20
2.2.4	Challenges in Photocatalytic CO ₂ Reduction with CH ₄	21
2.3	Progress in Photocatalytic CO ₂ Reduction with CH ₄	22
2.4	Recent Development in Titanium Dioxide (TiO ₂) Photocatalyst	25
2.5	Recent Development in Graphitic Carbon Nitrides (g-C ₃ N ₄) Photocatalyst	32
2.5.1	Structure and Properties of g-C ₃ N ₄	32
2.5.2	Thermodynamic Analysis of g-C ₃ N ₄	33
2.5.3	Synthesis of g-C ₃ N ₄	34
2.5.4	Modification of g-C ₃ N ₄ Photo-catalyst	37
2.5.4.1	Metals Modified g-C ₃ N ₄	38
2.5.4.2	Type II Heterojunction System	42
2.5.4.3	Z-scheme Heterojunction Systems	44
2.6	Development in Photocatalytic Reactors	49
2.6.1	Slurry Photoreactors	49
2.6.2	Fixed-bed Photoreactor	50
2.6.3	Annular Photoreactor	51
2.6.4	Optical Fiber Photoreactor	51
2.6.5	Monolith Photoreactor	53
2.7	Progress in Utilization of Monolith Photoreactor for CO ₂ Reduction	57
2.8	Kinetic Modelling	57
2.8.1	Fundamentals of Kinetic Study	57
2.8.2	Heterogeneous Photocatalysis Kinetic Study	60
2.8.3	Recent Developments in Photocatalysis Kinetic Models	62
2.9	Research Gap	64
CHAPTER 3	RESEARCH METHODOLOGY	66
3.1	Introduction	66
3.2	Research Materials and Gases	68

3.3	Synthesis of Photocatalysts	69
3.3.1	Preparation of g-C ₃ N ₄ and pCN Photocatalysts	71
3.3.2	Preparation of Ag/La-modified pCN Photocatalyst	71
3.3.3	Preparation of Ag-La-modified pCNNT Photocatalyst	72
3.3.4	Preparation of Ag-La/pCNNT Loaded Monolithic Honeycomb Support	73
3.3.5	Preparation of La/TiO ₂ Nanocatalyst	75
3.3.6	Synthesis of Ag-La-modified pCN-TiO ₂ Nanocomposites	76
3.4	Characterization of Materials	78
3.5	Experimental Setup	80
3.5.1	Design of Photoreactor System	80
3.5.1.1	Configuration of Fixed-bed Photoreactor	80
3.5.1.2	Configuration of Monolith Photoreactor	82
3.5.2	Procedure for Photocatalytic Activity	84
3.5.3	Gas Chromatography Analysis of Products	86
3.5.4	Study of Operating Parameters	87
3.6	Analysis of Experimental Data	89
3.6.1	Calculation of Crystal Size and Band Gap Energy	89
3.6.2	Calculation of Yield, Production Rate and Selectivity	90
3.6.3	Calculation of Quantum Efficiency	91
3.7	Photoinduced Chemical Reactions	92
3.8	Process Optimization and Kinetic Modelling	93
3.8.1	Process Parameters Optimization	93
3.8.2	Kinetic Study	93
CHAPTER 4	CHARACTERIZATIONS OF NANOMATERIALS	95
4.1	Introduction	95
4.2	X-ray Diffraction (XRD) Analysis	96

4.2.1	XRD Analysis of La-modified TiO ₂ Nanocatalyst	96
4.2.2	XRD Analysis of Ag/La Modified pCN Nanocatalysts	97
4.2.3	XRD Analysis of Ag/La-modified pCN-TiO ₂ Composites	99
4.3	Scanning Electron Microscopy (SEM) Analysis	102
4.3.1	SEM Analysis of La-modified TiO ₂ Nanocatalyst	102
4.3.2	SEM Analysis of Ag/La Modified pCN Nanocatalyst	102
4.3.3	SEM analysis of Ag/La-modified pCN-TiO ₂ composite catalyst	105
4.4	Transmission Electron Microscopy (TEM) Analysis	108
4.4.1	TEM Analysis of La-modified TiO ₂ Nanocatalyst	108
4.4.2	TEM Analysis of Ag/La Modified pCN Nanocatalyst	109
4.4.3	TEM Analysis of Ag/La-modified pCN-TiO ₂ Composites	110
4.5	N ₂ Adsorption-Desorption Analysis	112
4.5.1	BET Analysis of La-modified TiO ₂ Nanocatalyst	112
4.5.2	BET Analysis of Ag/La Modified pCN Nanocatalyst	114
4.5.3	BET Analysis of Ag/La-modified pCN-TiO ₂ Composites	116
4.6	UV-Visible Spectroscopic Analysis	119
4.6.1	UV-Visible Spectra of La Modified TiO ₂ Nanocatalyst	119
4.6.2	UV-Visible Spectra of Ag/La Modified pCN Photocatalyst	120
4.6.3	UV-Visible Spectra of Ag/La Modified pCN-TiO ₂ Composites	121
4.7	X-ray Photoelectron Spectroscopy (XPS) Analysis	123
4.7.1	XPS Analysis of La-modified TiO ₂ Nanocatalyst	123

4.7.2	XPS Analysis of Ag/La Modified pCNNT Nanocatalyst	125
4.7.3	XPS Analysis of Ag/La Modified pCN-TiO ₂ Composites	127
4.8	Photoluminescence (PL) Analysis	130
4.8.1	PL Analysis of La Modified TiO ₂ Nanocatalyst	130
4.8.2	PL Analysis of Ag/La Modified pCN Nanocatalyst	131
4.8.3	PL Analysis of Ag/La Modified pCN-TiO ₂ Composites	131
4.9	Chapter Summary	133
CHAPTER 5	PHOTOCATALYTIC CARBON DIOXIDE REDUCTION WITH METHANE AND WATER OVER TITANIA AND CARBON NITRIDE PHOTOCATALYSTS IN A FIXED-BED AND MONOLITH PHOTOREACTOR	136
5.1	Introduction	136
5.2	Photocatalytic CO ₂ Reduction with CH ₄ /H ₂ O Over La/TiO ₂ in a Fixed-Bed and Monolith Photoreactor	137
5.2.1	Effect of La-loading on TiO ₂ Photoactivity	137
5.2.2	Effect of Reaction Temperature On La/TiO ₂ Photoactivity	141
5.2.3	Effect of CH ₄ /H ₂ O Reductants on La/TiO ₂ Activity	144
5.2.4	Quantum Efficiency Analysis	148
5.2.5	Stability Analysis of La/TiO ₂ in a Fixed-bed and Monolith Photoreactor	151
5.3	Evaluation of Spent La/TiO ₂ Photocatalyst	152
5.4	Reaction Pathways in Photocatalytic CO ₂ Reduction with CH ₄ and H ₂ O	156
5.5	Photocatalytic CO ₂ Reduction with CH ₄ /H ₂ O over Ag/La Loaded pCN Photocatalyst in a Fixed-bed and Monolith Photoreactor	161
5.5.1	Photocatalytic CO ₂ Reduction with CH ₄ /H ₂ O Over Ag-La/pCN in a Fixed-bed Photoreactor	161
5.5.1.1	Effect of Protonation and Ag/La Loading on pCN Performance	161

5.5.1.2	Effect of Type of Light Irradiation and Reductant Type on Ag-La/pCNNT Photoactivity	163
5.5.1.3	Effect of Morphology on Ag-La/pCN and Ag-La/pCNNT Photoactivity	168
5.5.2	Performance of Ag-La/pCNNT Photocatalytic CO ₂ Reduction with CH ₄ /H ₂ O in a Monolith Photoreactor	170
5.5.3	Quantum Efficiency Analysis of Ag-La/pCNNT in a Fixed-bed and Monolith Photoreactor	173
5.6	Reaction Mechanism of Photo-induced CO ₂ Reduction with CH ₄ /H ₂ O over Ag-La-modified pCNNT Photocatalyst	175
5.7	Chapter Summary	178
CHAPTER 6	PHOTOCATALYTIC CARBON DIOXIDE REDUCTION WITH METHANE AND WATER OVER SILVER AND LANTHANUM MODIFIED CARBON NITRIDE AND TITANIUM DIOXIDE NANOCOMPOSITE	180
6.1	Introduction	180
6.2	Photocatalytic CO ₂ Reduction Over pCN-TiO ₂ Photocatalyst	181
6.3	Photocatalytic CO ₂ Reduction Over La-modified pCN-TiO ₂ Photocatalyst	183
6.3.1	Effects of La-loading on pCN-TiO ₂ Composite Photoactivity	183
6.3.2	Effects of UV and Visible Light Irradiations on La-modified pCN-TiO ₂ Composite Performance	185
6.3.3	Performance Comparison Between Fixed-bed and Monolith Photoreactor for Bireforming of Methane over La-modified pCN-TiO ₂ Composite	189
6.3.4	Stability Analysis of La-Modified pCN-TiO ₂ for BRM in a Monolith Photoreactor	191
6.4	Photocatalytic CO ₂ Reduction Over Ag-Modified pCN-TiO ₂ Photocatalyst	194
6.4.1	Effect of Ag-loading on the Performance of pCN-TiO ₂ Composite	194

6.4.2	Effect of UV AND Visible Light Irradiations On Performance of Ag-modified pCN-TiO ₂ Photocatalyst	196
6.4.3	Performance Comparison of Fixed-bed and Monolith Photoreactor for Photocatalytic BRM Over Ag-modified pCN-TiO ₂ Composite	198
6.4.4	Effect of Monolith Geometry On Photocatalytic BRM Reduction Over Ag-modified pCN-TiO ₂ Composite Photocatalyst	200
6.4.5	Effect of Reductants on Ag-Modified pCN-TiO ₂ in a Monolith Photoreactor	202
6.4.6	Stability Analysis of Ag-modified pCN-TiO ₂ Composite Photocatalyst in a Monolith Photoreactor	204
6.5	Photocatalytic CO ₂ Reduction over Ag/La Modified pCN-TiO ₂ Composite Photocatalyst in a Monolith Photoreactor	207
6.5.1	Effects of Ag/La Co-loading On the Photoactivity of pCN-TiO ₂ Composite	207
6.5.2	Effect of Reductant Types	209
6.5.3	Effect of Space Velocity	211
6.5.4	Effect of Feed ratios	214
6.5.5	Stability Analysis of Ag/La-modified pCN-TiO ₂ Composite Photocatalyst	216
6.6	Quantum Efficiency Analysis of Ag/La Modified pCN-TiO ₂ Composite	219
6.7	Reaction Mechanism for Bireforming of Methane Under UV and Visible Light Irradiations	224
6.6	Chapter Summary	228

CHAPTER 7	PARAMETERS OPTIMIZATION AND KINETIC MODELLING FOR PHOTOCATALYTIC BIREFORMING OF METHANE IN A MONOLITH PHOTOREACTOR	230
7.1	Introduction	230
7.2	Statistical Analysis Using RSM	231
7.2.1	Design of Experiments (DOE)	231
7.2.2	Model Fitting Analysis	234

7.3	Interaction Between Operating Parameters	243
7.3.1	Effect of processing parameters on CO Yield	243
7.3.1.1	Effect of Feed ratio on CO Yield	244
7.3.1.2	Effect of Temperature on CO Yield	247
7.3.1.3	Effect of Length on CO Yield	249
7.3.2	Effect of processing parameters on H ₂ Yield	250
7.3.2.1	Effect of Length on Production of H ₂	251
7.3.2.2	Effect of Temperature on Production of H ₂	253
7.3.2.3	Effect of Feed Ratio on Production of H ₂	256
7.3.3	Effect of Processing Parameters on C ₂ H ₆ Yield	258
7.4	Kinetic Study	261
7.4.1	Langmuir Hinshelwood Kinetic Modelling for BRM System	261
7.4.2	Validation of L-H Kinetic Model	266
7.5	Chapter Summary	272
CHAPTER 8	CONCLUSION AND RECOMMENDATIONS	2744
8.1	Research Outcomes	2744
8.2	Future Work	2766
	REFERENCES	2788
	APPENDICES A-D	303-313

LIST OF TABLES

TABLE NO.	TITLE	PAGE
Table 2.1	Summary of photocatalytic CO ₂ reduction with CH ₄ reduction over different semiconductor materials in different photocatalytic reactors	24
Table 2.2	Summary of literature on recent developments on photocatalysts for photocatalytic CO ₂ reduction with H ₂ O to fuels in different types of photoreactors	28
Table 2.3	Summary of literature on Metal Modified g-C ₃ N ₄ Photocatalysts	41
Table 2.4	Summary of literature on recent developments on heterojunction and Z-scheme Photocatalysts	47
Table 2.5	A summary of different types of reactors with their limitations [180, 198]	55
Table 3.1	Types and specification of chemicals used for catalyst synthesis	68
Table 3.2	Types of gases used during experimental work	69
Table 3.3	List of catalysts prepared with their compositions	70
Table 3.4	Temperature program applied for GC-system	86
Table 4.1	Cell parameters and crystallite sizes of TiO ₂ and La-modified TiO ₂ samples	97
Table 4.2	Summary of cell parameters and crystal volume of TiO ₂ in different Ag/La modified pCN-TiO ₂ composite samples	101
Table 4.3	Summary of physiochemical characteristics of TiO ₂ and La-modified TiO ₂ samples.	114
Table 4.4	The summary of surface area and pore volume of pCN and Ag-La-modified pCNNT samples	116
Table 4.5	The summary of surface area and pore volume of Ag-La-modified pCN-TiO ₂ samples	118
Table 4.6	Summary of XPS analysis of TiO ₂ and La-loaded TiO ₂ catalysts	124
Table 5.1	Summary of products yield at different La-doped TiO ₂ catalysts in a fixed-bed and monolith photoreactor	140

Table 5.2	Summary of Quantum Yield (%) for CO ₂ reduction with different reforming processes over 5 % La/TiO ₂ catalyst at 100 °C in a Fixed-bed and Monolith Photoreactor	150
Table 5.3	Summary of quantum yield (%) for CO ₂ reduction with different reforming processes over Ag-La-modified pCNNT catalyst	174
Table 6.1	Performance Comparison and Quantum Efficiency Analysis of Fixed-bed and Monolith Photoreactor for Photocatalytic Bireforming of Methane Under UV-light Irradiations	222
Table 6.2	Summary of literature on photocatalytic CO ₂ reduction with CH ₄ on different Photocatalysts	223
Table 7.1	Code Variables for 3 Level Factorial Design	231
Table 7.2	Full factorial CCD design matrix of independent variables along with experimental responses	233
Table 7.3	Coefficients of quadratic model for CO production ($R^2=0.8322$ and $R^2_{adj}=0.5806$, $MS_{residual}=303080.7$)	236
Table 7.4	Coefficients of quadratic model for H ₂ production ($R^2=0.7982$ and $R^2_{adj}=0.4957$, $MS_{residual}=1212558$)	237
Table 7.5	Coefficients of quadratic model for C ₂ H ₆ production ($R^2=0.7152$ and $R^2_{adj}=0.2881$, $MS_{residual}=14358$)	239
Table 7.6	ANOVA Table for the analysis of variance	241
Table 7.7	Summary of parameters after simulation of kinetic model for photocatalytic CO ₂ reduction with CH ₄ /H ₂ O over 3% Ag-5% La/pCN-TiO ₂ composite photocatalyst in a monolith photoreactor (Light intensity=150 mW/cm ²)	269
Table 7.8	Comparison of kinetic model constants with th50e reported values in literature for different CO ₂ reduction systems	271

LIST OF FIGURES

FIGURE NO.	TITLE	PAGE
Figure 2.1	Typical carbon dioxide conversion routes [73]	15
Figure 2.2	Difference in concepts of catalytic and photocatalytic reactions [83]	18
Figure 2.3	Surface charges pathways for photocatalytic oxidation-reduction processes over heterogeneous semiconductor photo-catalyst	19
Figure 2.4	(a) Triazine and (b) tri-s-triazine (heptazine) structures of g-C ₃ N ₄ [131]	33
Figure 2.5	Band gap energies of various semiconductor photocatalysts and selected redox potentials of H ₂ O splitting and CO ₂ reduction measured at pH 7 [83]	34
Figure 2.6	Schematic illustration of the synthesis process of g-C ₃ N ₄ by thermal polymerization of different precursors. The black, blue, white, red, and yellow balls denote C, N, H, O, and S atoms, respectively [131].	35
Figure 2.7	Reaction pathway for the development of g-C ₃ N ₄ using cyanamide as the precursor [131]	35
Figure 2.8	(a) XRD patterns of g-C ₃ N ₄ . TEM images of g-C ₃ N ₄ prepared at (b) 550 °C, (c) 600 °C, and (d) 650 °C. (e) UV-vis diffuse reflectance spectra and (f) transient photocurrent responses of g-C ₃ N ₄ developed at different calcination temperatures [131]	36
Figure 2.9	(a): Relationship between the pyrolysis duration and layer thickness of g-C ₃ N ₄ and the diagram for the layer-by-layer exfoliation and splitting mechanism of g-C ₃ N ₄ with decreased thickness and size. (b-g) TEM images of g-C ₃ N ₄ synthesized at 550 °C for (b-c) 0 min, (d-e) 60 min, and (f-g) 240 min [131]	37
Figure 2.10	Different strategies to improve performance of g-C ₃ N ₄ photocatalyst [150]	38
Figure 2.11	Schematic for energy band gaps and charge carrier's separation and transfer in Au/P-CN samples photocatalyst [139]	39
Figure 2.12	Production of various products over plasmonic Ag modified g-C ₃ N ₄ /TiO ₂ photo-catalysts [24]	43

Figure 2.13	Direct Z-scheme charge transfer mechanism for g-C ₃ N ₄ /SnS ₂ in photocatalytic reduction of CO ₂ [147]	45
Figure 2.14	A plausible mechanism for the selective photocatalytic reduction of CO ₂ to CH ₄ using g-C ₃ N ₄ /Ag-Ag ₃ PO ₄ photocatalyst under visible light irradiation [86]	45
Figure 2.15	Schematic presentation of different types of photoreactors: (a) Slurry reactor, (b) fixed-bed reactor, (c) annular type reactor, (d) optical fiber reactor [180]	52
Figure 2.16	(a) Schematic presentation of monolith reactor, (b) Cross section description of single channel, and (c) Heat and mass transfer process inside monolith channel [180]	54
Figure 2.17	Schematic representation of steps occurring during the mass transfer operation on the surface of photocatalyst [163]	59
Figure 2.18	Schematic of CO ₂ reduction with H ₂ O on heterogeneous photocatalyst: Adsorption-desorption process with surface reaction over catalyst surface based on the Langmuir-Hinshelwood mechanism [208]	62
Figure 3.1	Flowchart of general research methodology	67
Figure 3.2	Schematic presentation for the preparation of; (a) pristine pCN and (b) Ag-La modified pCN nanosheets	72
Figure 3.3	Schematic presentation for the preparation of Ag-La modified pCN nanotubes	74
Figure 3.4	Schematic of Ag-La-loaded carbon nitrides nanotubes (Ag-La/pCNNT) preparation and its coating over monolithic support	75
Figure 3.5	Schematic presentation for the synthesis of modified pCN-TiO ₂ Nanocomposite powder and supported over monolith channels	77
Figure 3.6	Experimental setup of fixed-bed photoreactor for photocatalytic CO ₂ reduction with CH ₄ /water mixture under simulated solar energy and UV-light irradiations	82
Figure 3.7	Experimental setup of monolith photoreactor for photocatalytic CO ₂ reduction with CH ₄ /water mixture under UV-light irradiations	84
Figure 4.1	XRD patterns of powder TiO ₂ and La-modified TiO ₂ samples	97
Figure 4.2	XRD patterns of pristine CN, pCN, Ag/pCN, La/pCN and Ag/La loaded pCNNT samples	98

Figure 4.3	(A) XRD analysis of Ag/La modified g-C ₃ N ₄ /TiO ₂ Catalysts: (a) TiO ₂ , (b) pCN, (c) pCN/TiO ₂ , (d) 5% Ag-pCN/TiO ₂ , (e) 5 % La-pCN/TiO ₂ , (f) 3% Ag-5% La/pCN/TiO ₂ ; (B) XRD analysis of samples coated over the monolithic support	100
Figure 4.4	SEM image of TiO ₂ and 5 wt. % La/TiO ₂ samples: (a) image of TiO ₂ NPs, (b) SEM image of 5 wt. % La/TiO ₂ nanoparticles, (c) EDX mapping analysis, (d) EDX plots of 5 wt. % La/TiO ₂ sample	103
Figure 4.5	SEM analysis of pristine CN, 5% Ag/pCN and 3% Ag-5% La-loaded pCNNT samples: (a) pristine CN, (b-c) 5% Ag/pCN, (d) 3% Ag-5% La loaded pCN, (e-f) 3% Ag-5% La/pCNNT samples	104
Figure 4.6	EDX mapping analysis of Ag-La/pCNNT sample, (a) Spectrum of Ag-La/pCNNT; (b) Mapping analysis of Ag-La/pCNNT with Ag-La distribution; (c) elements images; (d) EDX plots of 3 % Ag-5 % La/pCNNT sample	105
Figure 4.7	FESEM images of 3% Ag-5% La modified pCN-TiO ₂ composite under different magnifications: (a) SEM image of composite at 1.0 μm; (b-c) SEM images with uniform dispersion of pCN into TiO ₂ NPs obtained at 200 nm and (d) SEM image for uniform size TiO ₂ NPs and layered pCN sheets identified at 100 nm	106
Figure 4.8	SEM images of bare monoliths and 3 %Ag-5% La modified pCN-TiO ₂ composite catalysts coated over the monolithic supports: (a-b) bare channels and (c-d) catalyst coated over monolithic channels	107
Figure 4.9	TEM analysis of 5 wt. % La-modified TiO ₂ sample; (a and b) TEM images of TiO ₂ nanoparticles with uniform size and shape, (c) Image for d-spacing, (d) SAED patterns of 5 wt. %La/TiO ₂ sample	109
Figure 4.10	TEM images of pCN and 3 % Ag-5% La modified pCNNT samples: (a-b) bulk pCN, (c-d) bundle of pCN nanotubes, (e) Single pCN nanotube loaded with Ag-La NPs, (f) deposition of Ag-La NPs over pCN nanotube	111
Figure 4.11	TEM analysis of 3% Ag-5% La modified pCN-TiO ₂ composite catalyst: (a) bulk composite sample; (b-c) uniform dispersion of pCN with TiO ₂ NPs; (d) HRTEM image with d-spacing identification	112
Figure 4.12	Adsorption-desorption isotherms of TiO ₂ and La-modified TiO ₂ samples: (a) N ₂ adsorption-desorption isotherms, (b) Pore size distribution of corresponding samples	114

Figure 4.13	N ₂ adsorption desorption isotherms of CN and Ag-La modified pCNNT samples	115
Figure 4.14	(a) N ₂ adsorption-desorption isotherms of TiO ₂ , pCN and Ag/La modified pCN-TiO ₂ composite samples; (b) pore size distribution of corresponding samples	117
Figure 4.15	(a) UV-vis diffuse reflectance spectra of TiO ₂ and 5 wt. % La/TiO ₂ sample, (b) band gap energy of corresponding samples	119
Figure 4.16	(a) UV-Vis diffuse reflectance spectra of g-C ₃ N ₃ and La/Ag-loaded pCNNTs samples; (b) Plots of $(ah\nu)^2$ vs photon energy (eV) for band gap energy calculation	120
Figure 4.17	(a) UV-visible analysis of Ag-La modified pCN-TiO ₂ composite catalysts; (b) Plots of $(ah\nu)^2$ vs photon energy (eV) for band gap energy calculation	122
Figure 4.18	XPS analysis of 5 wt. % La modified TiO ₂ photocatalyst: (a) Ti 2p, (b) La 3d, (c) O 1s, (d) C 1s	124
Figure 4.19	XPS analysis of 3% Ag-5% La/pCNNTs catalyst: (a) wide spectra, (b) La3d, (c) Ag 3d, (d) N 1s, (e) O 1s and (f) C 1s	126
Figure 4.20	Calculation of VB position of Ag-La loaded pCNNT using XPS wide spectra	127
Figure 4.21	XPS analysis of Ag-La-Modified g-C ₃ N ₄ /TiO ₂ composite catalyst: (a) Ti; (b) Ag; (c) La; (d) O; (e) N; (f) C	129
Figure 4.22	Photoluminescence (PL) spectra of TiO ₂ and 5 wt. % La-loaded TiO ₂ nanoparticles	130
Figure 4.23	Photoluminescence analysis of g-C ₃ N ₄ and La/Ag-modified pCNNT samples	132
Figure 4.24	PL analysis of pCN, pCN-TiO ₂ , La/pCN-TiO ₂ , Ag/pCN-TiO ₂ and Ag-La Modified pCN-TiO ₂ samples	132
Figure 5.1	Effect of irradiation on the photo activity of TiO ₂ at different La-loading for CO ₂ reduction with CH ₄ to CO, H ₂ and hydrocarbons at 100 °C and CO ₂ /CH ₄ feed ratio 1.0: (a) CO production, (b) C ₂ H ₆ production and (c) H ₂ production	139
Figure 5.2	Effect of reaction temperature onto the photo-activity of 5 wt. % La/TiO ₂ NPs for CO ₂ reduction with CH ₄ to CO, H ₂ and C ₂ H ₆ at 100 °C at different irradiation time in a fixed-bed and monolith photoreactor; (a) production of CO, (b) production of H ₂ , (c) production of C ₂ H ₆	143
Figure 5.3	Effect of type of reducing system onto the photo-activity of 5 wt. % La/TiO ₂ NPs for CO ₂ reduction with CH ₄ to CO,	

	H ₂ and C ₂ H ₆ at 100 °C at different irradiation time; (a) production of CO, (b) production of H ₂ , (c) production of C ₂ H ₆ .	148
Figure 5.4	Stability analysis of 5 wt. %La/TiO ₂ in a continuous fixed-bed and monolith reactors for CO ₂ reduction with CH ₄ in presence of water: (a & c) fixed-bed photoreactor, (b & d) monolith photoreactor	152
Figure 5.5	TGA analysis of spent 5 wt. % La/TiO ₂ catalyst from fixed-bed and monolith photoreactors: (a) Analysis of fresh catalyst, (b) analysis of spent catalyst from fixed-bed reactor, (c) Analysis of spent catalyst from monolith reactor	154
Figure 5.6	EDX analysis of fresh and spent 5 wt. % La/TiO ₂ catalyst after 28 h of operation time for CO ₂ -CH ₄ reaction system: (a) SEM and EDX analysis of fresh catalyst, (b) SEM and EDX analysis of spent La/TiO ₂ catalyst from fixed-bed reactor, (c) SEM and EDX analysis of spent La/TiO ₂ catalyst from monolith reactor.	155
Figure 5.8	Schematic presentation of photocatalytic CO ₂ reduction with CH ₄ and H ₂ O to CO, H ₂ and hydrocarbons over 5 wt. % La-loaded TiO ₂ photocatalyst: (a) CH ₄ -H ₂ O reaction system, (b) CO ₂ -CH ₄ -H ₂ O reaction system.	159
Figure 5.9	(a) Schematic of the monolith photoreactor system, (b) Illustration of separation of electrons in the presence of La over the TiO ₂ surface, (c) Schematic presentation of photocatalytic CO ₂ reduction with CH ₄ /H ₂ O to CO and H ₂ over La-loaded TiO ₂ photocatalyst	160
Figure 5.10	Effect of Ag-La loading on the performance of pCN photocatalyst for CO ₂ reduction with CH ₄ in a fixed-bed reactor under visible light at temperature 100 °C and time 2 h: (a) effect of protonation; (b) Ag-loading, (b) La-loading, and (d) Ag-La loading to pCNNT: #S1 5 %Ag/pCN, #S2 5% La/pCN, #S3 1% Ag-5% La/pCNNT, #S4 3% Ag-5% La/pCNNT, #S5 5% Ag-5 % La/pCNNT.	162
Figure 5.11	Effect of type of reductants and types of light irradiation on the activity of 3% Ag-5%La-pCNNT for CO ₂ reduction in a continuous fixed-bed photoreactor at 100 °C and feed flow rate 5 mL/min: (a) Dry reforming of methane for CO and H ₂ production; (b) Bireforming of methane for CO and H ₂ production; (c) CH ₃ OH production in dry and bireforming of methane; (d) C ₂ H ₆ production in dry and bireforming of methane.	164
Figure 5.12	Performance mechanism of Ag-La/pCNNT for CO ₂ reduction with CH ₄ in the presence of H ₂ O under UV and	

	Visible light irradiations: (a) Efficiency enhancement due to visible light; (b) efficiency enhancement due to UV-light.	167
Figure 5.13	(a) Effect of morphology of Ag-La/pCN and Ag-La/pCNNT for photocatalytic CO ₂ reduction with CH ₄ in presence of H ₂ O under UV-light irradiation in a fixed-bed reactor and CH ₄ /CO ₂ feed ratio 1.0; (b) scheme of Ag-La pCN for performance analysis; (c) scheme of Ag-La pCNNT for reforming process.	169
Figure 5.14	Effect of reductants on the activity of 3% Ag-5% La loaded pCNNT for CO ₂ reduction with CH ₄ /H ₂ O system under UV-light in a continuous monolith photoreactor: (a) CO production; (b) H ₂ production; (c) CH ₃ OH production.	172
Figure 5.15	Schematic presentation of synergistic effects of Ag-La-loaded pCNNT for photocatalytic CO ₂ reduction with CH ₄ in presence of H ₂ O via BRM under UV/visible light irradiations	177
Figure 6.1	Effect of pCN-TiO ₂ ratio on photocatalytic CO ₂ reduction via bireforming of methane in a fixed-bed reactor under UV-light irradiations (Time=2 h, CO ₂ /CH ₄ =1.0, Catalyst=0.15 g)	183
Figure 6.2	Effect of La-loading on the performance of pCN-TiO ₂ for photocatalytic bireforming of methane in fixed-bed reactor; (Time=2 h, CO ₂ /CH ₄ =1.0, Catalyst=0.15 g, UV-light).	185
Figure 6.3	Photocatalytic bireforming of methane over La-modified pCN-TiO ₂ in a fixed-bed reactor under UV and Visible Light (CO ₂ /CH ₄ =1.0, Catalyst=0.15 g): (a) CO and H ₂ production under; (b) Hydrocarbons Production.	188
Figure 6.4	Photocatalytic bireforming of methane over La-modified pCN-TiO ₂ in a fixed-bed and monolith reactor; (a) CO and H ₂ production, (b) Hydrocarbons production (CO ₂ /CH ₄ =1.0, Flow=5 mL/min, UV-light)	190
Figure 6.5	Stability analysis of La-modified pCN-TiO ₂ for photocatalytic BRM in a monolith photoreactor under UV-light: (a) Yield of products; (b) H ₂ /CO ratio (CH ₄ /CO ₂ =1.0, Flow=5mL/min)	193
Figure 6.6	Effect of Ag-loading on the Performance of pCN-TiO ₂ for photocatalytic Bireforming of Methane in fixed-bed reactor; (Time=2 h, CO ₂ /CH ₄ =1.0, Catalyst=0.15 g).	195
Figure 6.7	Effect of Ag-modified pCN-TiO ₂ composite catalyst in CO ₂ reduction with CH ₄ /H ₂ O in a fixed-bed reactor under UV and visible light irradiations (Catalyst loading 0.15 g, CH ₄ /CO ₂ feed ratio 1.0)	197

Figure 6.8	Photocatalytic bireforming of methane over Ag-modified pCN-TiO ₂ in a Fixed-bed and monolith reactor: (a) CO and H ₂ production; (b) Hydrocarbons production (CH ₄ /CO ₂ ratio 1.0 and flow rate=5 mL/min)	199
Figure 6.9	Effect of monolith geometry in CO ₂ reduction with CH ₄ /H ₂ O over Ag-modified pCN-TiO ₂ composite under UV-light: (a) CO production; (b) H ₂ production; (c) C ₂ H ₆ production, (d) C ₂ H ₄ production (CH ₄ /CO ₂ 1.0, Flow=5 mL/min)	201
Figure 6.10	Effect of CH ₄ /H ₂ O reductants in photocatalytic CO ₂ reduction in a monolith photoreactor over Ag-modified pCN-TiO ₂ Nano catalyst: (a) CO production, (b) H ₂ production, (c) C ₂ H ₆ production, (d) C ₂ H ₄ production (CH ₄ /CO ₂ =1.0, Flow=5 mL/min)	203
Figure 6.11	Stability analysis of Ag-modified pCN-TiO ₂ composite photocatalyst for different reaction systems in a monolith photoreactor under UV-light irradiations: (a) Dry reforming of methane (CO ₂ -CH ₄); (b) Bireforming of methane (CO ₂ -CH ₄ -H ₂ O) (CH ₄ /CO ₂ =1.0, Flow=5 mL/min)	206
Figure 6.12	Effect of Ag and La on the performance of pCN-TiO ₂ for CO ₂ reduction with CH ₄ -H ₂ O in monolith photoreactor: (a) CO production; (b) H ₂ production, (c) C ₂ H ₆ production.	208
Figure 6.13	Effect of reductant types on the performance of Ag-La/pCN-TiO ₂ catalyst in monolith photoreactor under UV-light irradiations: (a) CO production, (b) H ₂ production, (c) C ₂ H ₆ production, (d) hydrocarbons production (CH ₄ /CO=1.0, Flow=5 mL/min)	211
Figure 6.14	Effect of feed flow rate on the performance of Ag-La/pCN-TiO ₂ catalyst for photocatalytic CO ₂ reduction with CH ₄ /H ₂ O in a monolith photoreactor under UV-light irradiations: (a) CO and H ₂ production; (b) Hydrocarbons production (CH ₄ /CO ₂ feed ratio of 1.0)	213
Figure 6.15	Effect of feed ratio on the performance of Ag-La modified pCN-TiO ₂ catalyst: (a) CO production; (b) H ₂ production.	215
Figure 6.16	Stability analysis of Ag-La-modified pCN-TiO ₂ nanocatalyst in a monolith photoreactor under UV-light irradiations for photocatalytic dry reforming and bireforming of methane: (a) Dry reforming of methane; (b) Bireforming of methane.	218
Figure 6.17	Type II heterojunction of Ag-La modified pCN-TiO ₂ composite catalysts for photocatalytic bireforming of methane under visible light irradiation	226

Figure 6.18	Direct Z-scheme Ag-La modified pCN-TiO ₂ composite catalysts for photocatalytic bireforming of methane under UV-light irradiations	227
Figure 6.19	Indirect Z-scheme Ag-La modified pCN-TiO ₂ composite catalysts for photocatalytic bireforming of methane under UV-light irradiations	228
Figure 7.1	Pareto-chart for developed regression models of dependent variables for CO production	236
Figure 7.2	Pareto-chart for developed regression models of dependent variables for H ₂ production	238
Figure 7.3	Plot of observed versus predicted values for C ₂ H ₆ production	239
Figure 7.4	The normal probability plot of the experimental results	244
Figure 7.5	Contour plot of CO production: interaction between temperature and monolith length at different feed ratios: (a) CH ₄ /CO ₂ =0.5; (b) CH ₄ /CO ₂ =2.0; (c) CH ₄ /CO ₂ =4.0.	246
Figure 7.6	Contour plot of CO production: interaction between CH ₄ /CO ₂ molar feed ratio and monolith length at different reaction temperature: (a) T=70 °C; (b) T=100 °C; (c) T=120 °C.	248
Figure 7.7	Contour plots of CO production: interaction between CH ₄ /CO ₂ molar feed ratio and temperature at different monolith lengths: (a) L=1 cm; (b) L=1.2 cm; (c) L=1.6 cm.	250
Figure 7.8	The normal probability plot of the experimental results	251
Figure 7.9	Contour plots of H ₂ production: interaction between CH ₄ /CO ₂ molar feed ratio and temperature at different monolith lengths: (a) L=1 cm; (b) L=1.2 cm; (c) L=1.6 cm	253
Figure 7.10	Contour plots of H ₂ production: interaction between CH ₄ /CO ₂ molar feed ratio and monolith length at different temperatures: (a) T=70 °C; (b) T=100 °C; (c) T=120 °C	255
Figure 7.11	Contour plots of H ₂ production: interaction between temperature and monolith length at different temperatures: (a) CH ₄ /CO ₂ =0.5; (b) CH ₄ /CO ₂ =2.0; (c) CH ₄ /CO ₂ =4.0	257
Figure 7.12	The normal probability plot of the experimental results	258
Figure 7.13	Contour plots of C ₂ H ₆ production: (a) interaction between temperature (X ₁) and feed ratio (X ₂); (b) interaction between feed ratio (X ₂) and length (X ₃); (c) interaction between temperature (X ₁) and monolith length (X ₃)	260

Figure 7.14	Schematic of CO ₂ reduction with CH ₄ /H ₂ O on heterogeneous photocatalyst: Adsorption-desorption process with surface reaction over catalyst surface based on the Langmuir-Hinshelwood mechanism	262
Figure 7.15	Plot of experimental data with model fitting for photocatalytic bireforming of methane for the production of CO over Ag-La/pCN-TiO ₂ photocatalyst in a monolith photoreactor applying different CH ₄ feed flow rates of 5, 10, 20, 30 and 40 mL/min at fixed CO ₂ feed flow rate (10 mL/min)	267
Figure 7.16	Plot of experimental data with model fitting for photocatalytic bireforming of methane for the production of H ₂ over Ag-La/pCN-TiO ₂ photocatalyst in a monolith photoreactor applying different CH ₄ feed flow rates of 5, 10, 20, 30 and 40 mL/min at fixed CO ₂ feed flow rate (10 mL/min)	268

LIST OF ABBREVIATIONS

BRM	-	Bireforming of Methane
CPSI	-	Channels Per Square Inch
CB	-	Conductance Band
DRM	-	Dry Reforming of Methane
F-T	-	Fischer-Tropsch
GHG	-	Greenhouse gas
L-H	-	Langmuir-Hinshelwood
LSPR	-	Localized Surface Plasmon Resonance
MFC	-	Mass flow controller
NHE	-	Normal Hydrogen Electrode
PL	-	Photoluminescence
pCNNT	-	Protonated Carbon Nitrides Nanotubes
pCN	-	Protonated Carbon Nitride
QE	-	Quantum Efficiency
SRM	-	Steam Reforming of Methane
VB	-	Valence Band

LIST OF SYMBOLS

α	-	Absorption coefficient
β	-	Full peak width at half maximum
c	-	Speed of light
d_h	-	Channel size
D	-	Average particle size
E_F	-	Fermi level
e^-	-	Electron
E_{bg}	-	Energy band gap
E	-	Activation energy
E_p	-	Energy of photon
f	-	Photon flux
h	-	Plank constant
ΔH	-	Change in enthalpy of reaction (kJ/mole)
h^+	-	Hole
H	-	Heat of reaction
I	-	Irradiance
L	-	Thickness of crystallite (nm)
λ	-	X-ray wavelength
θ	-	Braggs angle

LIST OF APPENDICES

APPENDIX	TITLE	PAGE
Appendix A	List of Publications	305
Appendix B	Photographs of Accessories and Reactors	307
Appendix C	Photographs of Monolithic Support and Nanocatalysts	307
Appendix D	Chromatographs and Products Analysis	307

CHAPTER 1

INTRODUCTION

1.1 Background Overview

Global warming effects due to greenhouse gases, primarily carbon dioxide (CO₂) and methane (CH₄) emitted due to fossil fuel combustion and human activities are prevalent [1]. The emission reduction of CO₂ for cleaner environment can be categorized into three routes which include direct reduction of CO₂ emission from the source [2], CO₂ capture and storage (CCS) and utilization of CO₂. The direct CO₂ emission at the source can be reduced using renewable energy resources that produces lesser CO₂ [3], but these energy sources are limited compared to fossil fuels [4]. CO₂ capture and storage is a technology that is being developed to allow CO₂ emissions from fossil fuel, capture at large point sources to be transported to safe geological storage, rather than being emitted to the atmosphere [5]. CCS disadvantage is the extra cost to transport and injection to the geological storage. Besides, due to industrialization integrated with daily human activities caused the increase of fossil fuels combustion; thus mitigating CO₂ emission and/or storage for sustainable development is unachievable [6]. Therefore, utilization of CO₂ to produce chemicals and fuels is the growing concern in recent years [7].

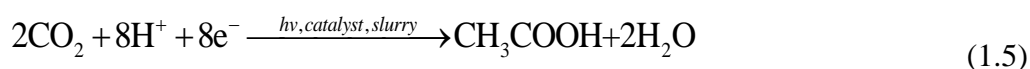
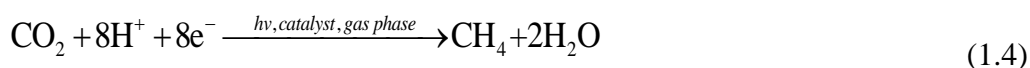
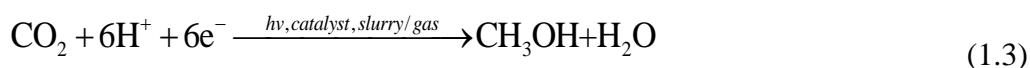
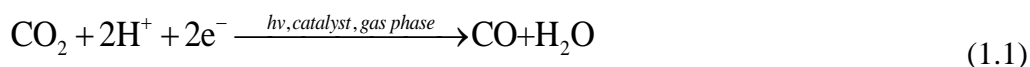
Among the available CO₂ utilization approaches, the most widely employed technologies are thermal and plasma processes. In thermal process, CO₂ can be converted through an endothermic process by providing an input energy at elevated temperature. However, higher temperature makes this process expensive and has adverse effect on the catalyst stability, while coke produced ultimately deactivates the catalyst [8]. On the other hand, plasma technology for dry reforming of methane is considered better alternatives compared to thermal process. The plasma reforming has advantages of high conversion because reactions are conducted by electron induced chemistry. However, production of large amounts of coke during dry reforming of

methane in plasma reactor is a great challenge. In addition, higher input energy is required to generate plasma, which make this process un-economical [9-11].

In recent innovations, phototechnology has gained much attention because it works in the presence of light irradiations. Using photocatalysis, CO₂ reforming of CH₄ would be possible at normal temperature and atmospheric pressure [12]. The requirement of input energy as like endothermic process can be provided through harvesting solar energy. More importantly, catalyst can be used with prolonged stability due to mild operating conditions, while economical production of chemicals and fuels.

1.2 Photocatalytic CO₂ Reforming of CH₄

Photocatalytic reduction of CO₂ seems a potential technology to produce chemicals and fuels at normal operating conditions with the help of light irradiations. During the past three decades, photocatalytic reduction of CO₂ over various semiconductor materials has been investigated by many researchers and products reported were carbon monoxide (CO), methane (CH₄), methanol (CH₃OH), formic acid (HCOOH) and acetic acid (CH₃COOH) as discussed in Equations (1.1) to (1.5) [13-16].



Since 1980s, water as a reductant for the reduction of CO₂ in a gas phase and slurry system, has attracted considerable interest with diversity of products (e.g., CO,

CH₄, H₂, CH₃OH, HCOOH and HCHO) [13-16]. Using gas phase system, CO₂ with water can be converted to CO, CH₄ and CH₃OH as the potential products. However, slurry system promoted the production of CH₃OH, HCHO and CHOOH during CO₂ reduction with H₂O [17]. In this perspective, production of CH₄ from photo-reduction of CO₂ with water vapours over Fe/TiO₂ [18], photo-reduction of CO₂ with H₂O to liquid products (CH₃OH, HCHO) over CeO/TiO₂ [19], use of Ag-MgO/TiO₂ for the production of CH₄ from CO₂ and water in gas phase system [20], Fe-doped CeO for CO and CH₄ production from CO₂ and water vapours [21], production of CO from CO₂-water vapours over Ag/CdS [22], Ag/TiO₂ nanorods [23], g-C₃N₄/Ag/TiO₂ composite catalyst for the production of CO and CH₄ from CO₂-water [24], production of CO from CO₂-water using g-C₃N₄/N/TiO₂ catalyst [25] and g-C₃N₄/Cu/TiO₂ for the production of CH₃OH, HCHO and HCOOH from CO₂ in slurry system [26], have been reported.

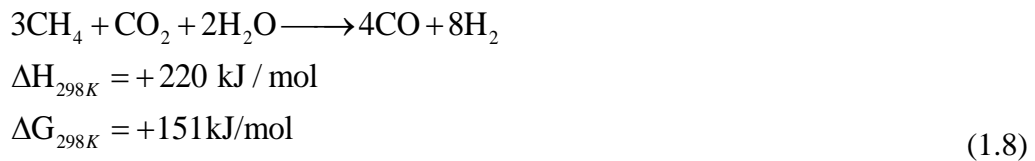
Although, different types of photocatalysts with appreciable improvement in CO₂ reduction to fuels has been succeeded by numerous researchers, but main challenge is diversity of products distribution. In addition, research on utilization of both greenhouse gases (CO₂ and CH₄) is still relevant. CH₄ is emitting from gas supply chain [27], landfill [28] and industries, is a severe challenge for the future. Therefore, recycling both greenhouse gases (CO₂ and CH₄) to valuable chemicals and fuels by reforming deems an attractive pathway for a cleaner environment. CO₂ reforming is a method of producing synthesis gas (syngas), a mixture of CO and H₂, from the mixture of CO₂ and hydrocarbons, in particular, methane. Conventionally, syngas is produced via dry reforming of methane. The reforming of CO₂ and CH₄ is a challenging task as both are stable molecules, while reforming of these two molecules to syngas is an endothermic process that demands excessive supply of energy [29, 30]. However, it is a main raw material in the production of liquid fuels. Besides, syngas (H₂/CO) ratio for the production of liquid fuels has great importance, e.g., a ratio of H₂/CO of 2 would be required in methanol synthesis process.

Methane can be converted into syngas through different reforming technologies such as steam reforming of methane (SRM) as shown in Equation (1.6). CO₂ can also be utilized with CH₄ for the production of syngas through catalytic CO₂

and CH₄ reforming or dry reforming of methane (DRM) as explained in Equation (1.7) [31]. DRM offers advantages such as mitigating both greenhouse gases, and direct production of syngas [32]. However, DRM operates under higher temperature via thermal reforming is prone to coking and reduces catalyst stability [33].



Combination of SRM and DRM also known as bireforming of methane (BRM) could be a promising approach and interesting pathway for the production of H₂ enriched syngas as explained in Equation (1.8) [34]. BRM has advantage over SRM and DRM for producing hydrogen with a stoichiometric H₂/CO ratio of 2, a more favourable composition for the production of liquid fuels via Fischer-Tropsch Synthesis (FTS) [35]. Although, BRM is an attractive approach compared to DRM, yet it also requires larger input energy due to endothermic process [36].



With the help of phototechnology, reforming processes can be conducted at normal temperature and atmospheric pressure. However, there are limited reports available on photocatalytic CO₂ reduction with CH₄ through phototechnology. Recently, photocatalytic CO₂ reforming of CH₄ to fuels over different semiconductor photocatalysts has been reported [37, 38]. In one of the earlier studies, Shi et al. [39] reported photocatalytic CO₂ reduction with CH₄ over Cu/CdS modified TiO₂/SiO₂ photocatalyst in a fixed-bed photoreactor operating at high temperature. Products obtained were C₂H₆, CH₃COOH, CH₃COCH₃ and CO. ZrO₂ photocatalyst was employed for CO₂-CH₄ reduction under UV-light with the production of CO and H₂

as the main products [40]. Similarly, CO and H₂ were produced during CO₂ reduction with CH₄ over Pt-loaded TiO₂ and Au/Rh loaded TNTs catalyst, respectively [41]. However, literature on photocatalytic CO₂ reduction with CH₄ in the presence of H₂O via BRM is not available. Besides, ubiquitous TiO₂ is mainly employed as a photocatalyst in CO₂ reforming of CH₄, but the production rate was not much appreciable. Lower TiO₂ photoactivity attributing to poor CO₂ adsorption due to acid nature and fast photogenerated charges recombination rate.

Significant research has been conducted on developing efficient photocatalysts, while the use of basic oxide in TiO₂ is considered as one prospect to promote CO₂ adsorption. In recent years, rare-earth metals are typically investigated for the modification of TiO₂ structure to enable the increment of surface oxygen vacancies [42]. Lanthanum (La), due to the unique electronic configuration and spectral characteristics, is considered as the best dopant for modifying crystal structure, optical properties and surface adsorption of TiO₂ [43, 44]. Li et al., [45] reported the use of La as an efficient metal for selective photocatalytic CO₂ reduction with H₂O to CH₄ under UV-light. The enhanced and selective photoactivity of La/TiO₂ photocatalyst was due to higher CO₂ adsorption because of its surface basicity with proficient charge separation. Similarly, silver (Ag) metal is gaining large interest due to its appropriate work function (W_s) for photocatalytic applications [46, 47]. Many research articles reported the use of Ag based semiconductors for selective CO₂ photoreduction during photocatalytic CO₂ reduction with H₂O under UV and visible light irradiations [48-52].

Recently, graphitic carbon nitride (g-C₃N₄) semiconductor is considered very promising for CO₂ reduction applications. This is because of its merits of low-cost preparation, high chemical stability and possessing appropriate electronic structure with medium band gap energy (2.70 eV) [53, 54]. Nevertheless, photoactivity of the pure g-C₃N₄ is still limited due to fast charges recombination rate [55]. Many attempts have been employed to increase the performance of g-C₃N₄ such as surface charge modification, designating an appropriate textural porosity, metal doping, non-metal doping and coupling with other semiconductors [26, 56]. Ong and co-workers reported the surface charge modification of g-C₃N₄ via protonation with enhanced photo-

activity for CO₂ reduction to CH₄ [57]. In another work, g-C₃N₄ loaded with Pt for enhanced CH₄ production during photocatalytic CO₂ reduction has been reported [58]. CeO₂ loaded into g-C₃N₄ remarkably enhanced photocatalytic activity for CO₂ reduction by H₂O to CO and CH₄ [59]. Similarly, Ag-loaded-gC₃N₄ has been investigated for selective H₂ production as Ag suppressed the recombination of charge carriers [49, 60].

In the recent development, fabrication of semiconductors heterojunctions or Z-scheme photo-catalysts are considering more significant due to efficient charges separation with the adjustment of band structure for selective CO₂ reduction to fuels. In this perspective, CO₂ photoreduction with H₂O to CH₃OH was tested using g-C₃N₄/Cu/TiO₂ as a photo-catalyst [26]. In another work, indirect Z-scheme BiOI/g-C₃N₄ was investigated for visible light driven CO₂ reduction with H₂O with the production of CO, H₂ and CH₄ [61]. The selective photocatalytic CO₂ reduction with H₂O over g-C₃N₄-N/TiO₂ [62], ZnV₂O₆/g-C₃N₄ [63] and Mg-gC₃N₄ [64] composites have been investigated. Similarly, Ag-loaded g-C₃N₄/TiO₂ for CO₂ photo-reduction by H₂O to fuels was explored [24]. g-C₃N₄ is widely investigated in photocatalytic CO₂ reduction with H₂O, but not for CO₂-CH₄ reaction system via DRM and BRM. The efficiency of g-C₃N₄ can be further improved through surface charge modification via protonation [63]. Besides, development of Ag/La modified Z-scheme g-C₃N₄/TiO₂ composite would be promising for enhanced photocatalytic dry and bireforming of methane.

Upscaling CO₂ reforming of CH₄ system to synthesis gas (CO and H₂) requires stringent criteria for designing the photoreactor system. The choice of reactor is critical since it affects the overall CO₂ reduction efficiency and products selectivity. Almost all photoinduced CO₂-methane reaction systems were conducted in a fixed-bed photoreactor, where catalysts are distributed over the reactor surface. The fixed-bed reactors have limitations: (1) poor light utilization efficiency due to less exposed active surface area; (2) lower adsorption- desorption process due to less contact of gas with catalyst; (3) smaller catalyst loading and (4) less light intensity to stimulate complex nature of CO₂-CH₄ photocatalytic reaction [65]. Therefore, the design of highly

efficient photoreactor for CO₂-CH₄ reduction is crucial to scale up phototechnology from laboratory to commercial level.

More recently, the attention on immobilized photocatalytic systems with enhanced light utilization efficiency has surged [66, 67]. Among the different supports, monolithic substrates are mainly studied because of the unique structure, higher adsorption-desorption process, larger active surface area, more catalyst loading, controlled selectivity and large photonic efficiency [66, 68]. In this perspective, monolith photoreactor found very efficient for photocatalytic CO₂ reduction to CO with enhanced selectivity and yield using H₂O and H₂ reductants over different types of semiconductor materials [48, 69].

The focus of this study is to design and develop structured Ag/La modified g-C₃N₄-TiO₂ nanocomposite for photocatalytic dry and bireforming of methane in a monolith photoreactor. The coupling TiO₂ and g-C₃N₄ will be suitable for Z-scheme photocatalytic reactions under UV-light and direct heterojunction electron transfer under visible light. The modification of g-C₃N₄/TiO₂ with La/Ag metals will develop novel polymeric complexes that would maximize the process efficiency under UV and visible light irradiations. The use of water in dry reforming of methane would be suitable for the production of hydrogen enrich syngas. The monolith photoreactor will maximize the illuminated surface area even at lower light intensity, thus increasing the efficiency of reactor system for CO₂ photo-reduction to hydrogen enrich syngas. The optimization of different operating parameters and kinetic investigation will further improve the system efficiency.

1.3 Problem Statement

The conversion of greenhouse gases i.e., CH₄ and CO₂ to renewable fuels has become a challenge to achieve net-zero carbon cycle for monitoring energy crises and environment pollution. The breaking stable molecules of CH₄ and CO₂ demands higher input energy, while overcoming this barrier through external supply of energy makes

this process uneconomical. The main challenges for the conversions of greenhouses to chemicals and fuels are as follows:

1. Thermal process requires higher input energy to break stable CO₂ and CH₄ molecules. The energy barrier for recycling CO₂ and CH₄ can be resolved using phototechnology, yet limited reports are available on photocatalytic CO₂ reduction with CH₄. The lower production rate during photocatalytic conversion of CO₂ and CH₄ with diversity of products is another barrier in the use of phototechnology;
2. Among the semiconductors, TiO₂ and metal modified TiO₂ photocatalysts have been investigated for CO₂ reforming of CH₄. However, TiO₂ yielded lower photo-activity due to faster charges recombination and inappropriate redox potentials. This urges to find new and highly efficient composite photocatalyst for selectivity DRM process under UV and visible light irradiations. Recently, g-C₃N₄ has been investigated for CO₂ reduction with H₂O applications, however, it has not been reported in DRM and BRM applications;
3. The production of synthesis gas with higher H₂/CO ratio in another challenge in photocatalytic dry reforming of methane process. This is because, during photocatalytic CO₂ reduction with CH₄, diversity of products has been reported;
4. Besides, photoreactors investigated are fixed-bed which have lower quantum efficiency. These reactors are not very efficient due to inefficient light distribution and have minimum surface area for carrying catalytic reactions.

1.4 Research Hypothesis

The lower CO₂ conversion efficiency and production rates through phototechnology can be improved by employing an efficient reducing agent, photocatalyst and photoreactor. Therefore, the followings are the research hypothesis:

1. Although, both CO₂ and CH₄ are very stable molecules, yet CO₂ and CH₄ can be converted to chemicals using phototechnology. The problem of lower TiO₂ photoactivity can be resolved by loading with basic oxide materials, in particular lanthanum (La). Basic oxides would be helpful to improve CO₂ adsorption and will promote charges separation.
2. The use of graphitic carbon nitride (g-C₃N₄) would be promising in photocatalytic CO₂ reduction with CH₄ due to its visible light response, appropriate band structure and low-cost synthesis. The surface charge modification and addition of metals such as Ag and La metals would be promising to improve efficiency and selectivity for synthesis gas production;
3. Coupling g-C₃N₄ with TiO₂ will provide appropriate band structure with efficient charges separation and would enable efficient reduction of CO₂ with CH₄ under UV and visible light irradiations. For this purpose, direct heterojunction of g-C₃N₄/TiO₂ for visible light and Z-scheme g-C₃N₄/TiO₂ nanocomposites would be promising for UV-light applications. The efficiency of composite will be further improved by loading with Ag and La metals, thus would be helpful to improve photoactivity and selectivity;
4. Composition of synthesis gas can be adjusted using different reforming technologies. The lower H₂/CO ratio in synthesis gas during CO₂ reduction with CH₄ can be improved by combining DRM process with steam reforming of methane (SRM). Thus, photocatalytic CO₂ reduction with CH₄ in the presence of H₂O via bireforming of methane (BRM) would be promising to get higher production rate and selectivity;
5. The lower quantum efficiency of photoreactor system because of inefficient light distribution over the catalyst surface is intended to overcome employing monolith photoreactor. The monolith photoreactor will be productive to provide larger illuminated active surface area, higher adsorption-desorption and efficient mass transfer toward the catalyst surface. Higher light distribution and harvesting over the catalyst surface would also be possible utilizing micro-channels, ultimately stimulating higher quantum efficiency toward efficient reduction of CO₂ with CH₄/water system;

6. The effect of different parameters and their optimization would also be helpful to improve production rate and products selectivity. The kinetic study will further provide insights about the photon flux utilization and reaction rate limitations.

1.5 Research Objectives

The objectives of this research are:

- (a) To synthesize and characterize Ag/La modified g-C₃N₄-TiO₂ nanocomposite photocatalysts functional under UV and visible light irradiations;
- (b) To study the performance of composite nanocatalysts for photocatalytic CO₂ reduction with CH₄/H₂O through dry and bireforming of methane under UV and visible light irradiations;
- (c) To compare quantum performance of fixed-bed with a monolith photoreactor for photocatalytic CO₂ reduction with CH₄/H₂O through dry and bireforming of methane;
- (d) To investigate effect of process parameters on photocatalytic bireforming of methane over composite photocatalyst in a monolith photoreactor;
- (e) To optimize process parameters using response surface methodology and develop kinetic model to determine reaction rate parameters in photocatalytic bireforming of methane.

1.6 Research Scope

This study focused on determining some mechanistic and fundamental problems pertaining to lower CO₂ and CH₄ reduction efficiency and products selectivity. The fabrication of plasmonic and polymeric nanocatalysts with various metals and co-metals loading into pCN and pCN-TiO₂ nanostructures has been

inspected. The effects of operating parameters on CO₂ reduction such as metal-doping levels, feed ratios, and reaction temperature and irradiation times is also deliberated. The performance analysis of a monolith with a fixed-bed photoreactors has been investigated to get higher yield and selectivity. The reaction mechanisms of CO₂ reduction and CH₄/water oxidation and quantum efficiency analysis has been deliberated. The CO₂ reduction efficiency is related to maximize yield of desired products. Therefore, the specific research scope of this study is as follows:

1. The catalysts such as TiO₂, pCN pCN-TiO₂, Ag-La/pCNNT and Ag/La modified pCN-TiO₂ are synthesized using sol-gel and hydrothermal methods to investigate the route of CO₂ reduction with CH₄/H₂O. The optimized materials are supported over the monolith channels using sol-gel dip-coating method. The catalysts are characterized using XRD, SEM, FESEM, HRTEM, BET, XPS, UV-Visible and PL spectroscopy. This was helpful to investigate crystallinity, phase, morphology, surface area, pore size distribution, metals transition states and optical properties.
2. The performance of catalysts for photochemical reduction of CO₂ with CH₄/H₂O is investigated using photocatalytic steam reforming of methane (SRM), photocatalytic dry reforming of methane (DRM) and photocatalytic bireforming of methane (BRM) under UV and visible light irradiations. The role of each catalysts is critically evaluated to understand their impacts on the products yield and selectivity in the presence of different reforming processes and light systems.
3. The photoreactors employed are fixed bed and monolith of multiple channels. The quantum performance of both photoreactors is investigated using different reforming systems (i.e., SRM, DRM and BRM) under UV and visible light irradiations. In a fixed bed, photocatalysts are distributed at the reactor bottom, however, they are coated inside monolith microchannels using sol-gel dip-coating method. The mass flow controllers are employed to adjust feed flow rates and feed ratios in different reaction system. A reflector type 200W Hg lamp is used as a source of UV-light irradiations with intensity 150 mW/cm² and wavelength 254 nm. A solar simulator is used as a source of visible light

irradiations with intensity equal to 100 mW/cm^2 . More importantly, solar arrays with batteries are installed to provide input electricity for the operation of both photoreactors.

4. The operating parameters investigated are reaction temperature, feed ratios, and monolith geometry and irradiation time. The reaction mechanism is developed to find out key parameters in CO_2 reduction applications for different reforming systems under UV and visible light irradiations.
5. The optimization of process parameters is carried out using response surface methodology (RSM). The kinetic model is developed using Langmuir-Hinshelwood mechanism and rate constants are determined.

1.7 Research Significance

Greenhouse gas CO_2 is efficiently reduced with CH_4 for synthesis gas (CO , H_2) production in the presence of different photo-catalytic systems. The monolith photoreactor performance is very encouraging while the efficiency found was much higher compared to fixed-bed photoreactor. The composite catalysts are highly productive for CO_2 and CH_4 reduction to syngas gas. The several outcomes of this research are described below:

- (a) A new route for photocatalytic CO_2 reduction with CH_4 through dry reforming of methane (DRM) and bireforming of methane (BRM) reactions.
- (b) Development of microchannel monolith photoreactor system to investigate efficient photocatalytic DRM and BRM for synthesis gas production.
- (c) New methods and findings on the synthesis of protonated graphitic carbon nitrides nanotubes and z-scheme composite catalysts.
- (d) Low-carbon economy shift through CO_2 recycling.
- (e) Alternative solutions to energy crises and global warming.

1.8 Layout of Thesis

The research is focused on the photocatalytic CO₂ reduction with CH₄ through dry reforming of methane and biforming of methane over Ag or La doped and Ag-La co-doped pCN-TiO₂ composite nanocatalyst in a fixed-bed and continuous mode operation of monolith photoreactor. The development of Ag-La modified pCN-TiO₂ nanocatalyst suitable for efficient CO₂ reduction via DM and BRM with H₂/CO and hydrocarbon fuels has been investigated. The synthesis and characterization of materials, optimization of metals loading, investigation of operating parameters, and evaluation of reactor performances for higher production rate and reaction mechanisms are discussed in different chapters. This thesis consists of eight chapters.

Background of the research and problem at hand, research hypothesis, objectives and scope of this study are discussed in Chapter 1. Chapter 2 presents literature survey pertaining to possible pathways for CO₂ recycling, fundamentals and progress in CO₂ reduction to hydrocarbon fuels, progress in CO₂ reduction with CH₄ over different photo-catalysts, selection of photo-catalysts, and description of photocatalytic reactors. In Chapter 3, general description of research methodology and detailed experimental strategies are discussed. The characterizations of nanocatalysts are discussed in Chapter 4. Performance analysis of metals modified TiO₂ and pCN in a fixed-bed and monolith photoreactor for photocatalytic CO₂ reduction with CH₄/H₂O is presented in Chapter 5. Chapter 6 investigates the photocatalytic CO₂ reduction via BRM over Ag-La modified pCN-TiO₂ catalysts in a microchannel monolith photoreactor under UV-light irradiations. The optimization of process parameters using response surface methodology and kinetic model development has been presented in Chapter 7. Finally, Chapter 8 contains the overall conclusions of this study and recommendations for future work.

REFERENCES

1. Pao, H.-T. and C.-C. Chen, Decoupling strategies: CO₂ emissions, energy resources, and economic growth in the Group of Twenty. *J. Cleaner Prod.*, 2019. 206:907-919.
2. Mardoyan, A. and P. Braun, Analysis of Czech Subsidies for Solid Biofuels. *Int. J. Green Energy*, 2014. 12(4):405-408.
3. Roy, S.C., O.K. Varghese, M. Paulose, and C.A. Grimes, Toward solar fuels: photocatalytic conversion of carbon dioxide to hydrocarbons. *Acs Nano*, 2010. 4(3):1259-1278.
4. Menanteau, P., D. Finon, and M.-L. Lamy, Prices versus quantities: choosing policies for promoting the development of renewable energy. *Energy policy*, 2003. 31(8):799-812.
5. Bachu, S., Screening and ranking of sedimentary basins for sequestration of CO₂ in geological media in response to climate change. *Environ. Geol.*, 2003. 44(3):277-289.
6. Alaba, P.A., A. Abbas, and W.M.W. Daud, Insight into catalytic reduction of CO₂: Catalysis and reactor design. *J. Cleaner Prod.*, 2017. 140:1298-1312.
7. Tahir, M., B. Tahir, and N.S. Amin, Photocatalytic CO₂ reduction by CH₄ over montmorillonite modified TiO₂ nanocomposites in a continuous monolith photoreactor. *Mater. Res. Bull.*, 2015. 63:13-23.
8. Lee, H.Y., A.R. Kim, M.-J. Park, J.M. Jo, D.H. Lee, and J.W. Bae, Combined steam and CO₂ reforming of CH₄ using coke oven gas on nickel-based catalyst: Effects of organic acids to nickel dispersion and activity. *Chem. Engin. J.*, 2015. 280:771-781.
9. Tao, X., M. Bai, X. Li, H. Long, S. Shang, Y. Yin, and X. Dai, CH₄-CO₂ reforming by plasma - challenges and opportunities. *Prog. Energy Combust. Sci.*, 2011. 37(2):113-124.
10. Long, H., S. Shang, X. Tao, Y. Yin, and X. Dai, CO₂ reforming of CH₄ by combination of cold plasma jet and Ni/[gamma]-Al₂O₃ catalyst. *Int. J. Hydrogen Energy*, 2008. 33(20):5510-5515.

11. Li, D., X. Li, M. Bai, X. Tao, S. Shang, X. Dai, and Y. Yin, CO₂ reforming of CH₄ by atmospheric pressure glow discharge plasma: A high conversion ability. *Int. J. Hydrogen Energy*, 2009. 34(1):308-313.
12. Díaz Alvarado, F. and F. Gracia, Steam reforming of ethanol for hydrogen production: Thermodynamic analysis including different carbon deposits representation. *Chem. Eng. J.*, 2010. 165(2):649-657.
13. Olivo, A., V. Trevisan, E. Ghedini, F. Pinna, C.L. Bianchi, A. Naldoni, G. Cruciani, and M. Signoretto, CO₂ photoreduction with water: Catalyst and process investigation. *J. CO₂ Util.*, 2015. 12:86-94.
14. Chang, X., T. Wang, and J. Gong, CO₂ photo-reduction: insights into CO₂ activation and reaction on surfaces of photocatalysts. *Energy Environ. Sci.*, 2016. 9(7):2177-2196.
15. Abdullah, H., M.M.R. Khan, H.R. Ong, and Z. Yaakob, Modified TiO₂ photocatalyst for CO₂ photocatalytic reduction: An overview. *J. CO₂ Util.*, 2017. 22:15-32.
16. Sohn, Y., W. Huang, and F. Taghipour, Recent progress and perspectives in the photocatalytic CO₂ reduction of Ti-oxide-based nanomaterials. *Appl. Surf. Sci.*, 2017. 396:1696-1711.
17. Karamian, E. and S. Sharifnia, On the general mechanism of photocatalytic reduction of CO₂. *J. CO₂ Util.*, 2016. 16:194-203.
18. Do, J.Y., Y. Im, B.S. Kwak, J.-Y. Kim, and M. Kang, Dramatic CO₂ photoreduction with H₂O vapors for CH₄ production using the TiO₂ (bottom)/Fe–TiO₂ (top) double-layered films. *Chem. Eng. J.*, 2015. 275:288-297.
19. Xiong, Z., Y. Zhao, J. Zhang, and C. Zheng, Efficient photocatalytic reduction of CO₂ into liquid products over cerium doped titania nanoparticles synthesized by a sol–gel auto-ignited method. *Fuel Process. Technol.*, 2015. 135:6-13.
20. Li, H., X. Wu, J. Wang, Y. Gao, L. Li, and K. Shih, Enhanced activity of AgMgOTiO₂ catalyst for photocatalytic conversion of CO₂ and H₂O into CH₄. *Int. J. Hydrogen Energy*, 2016. 41(20):8479-8488.
21. Wang, Y., F. Wang, Y. Chen, D. Zhang, B. Li, S. Kang, X. Li, and L. Cui, Enhanced photocatalytic performance of ordered mesoporous Fe-doped CeO₂

- catalysts for the reduction of CO₂ with H₂O under simulated solar irradiation. *Appl. Catal. B: Environ.*, 2014. 147:602-609.
22. Zhu, Z., J. Qin, M. Jiang, Z. Ding, and Y. Hou, Enhanced selective photocatalytic CO₂ reduction into CO over Ag/CdS nanocomposites under visible light. *Appl. Surf. Sci.*, 2017. 391:572-579.
 23. Cheng, X., P. Dong, Z. Huang, Y. Zhang, Y. Chen, X. Nie, and X. Zhang, Green synthesis of plasmonic Ag nanoparticles anchored TiO₂ nanorod arrays using cold plasma for visible-light-driven photocatalytic reduction of CO₂. *J. CO₂ Util.*, 2017. 20:200-207.
 24. Li, H., Y. Gao, X. Wu, P.-H. Lee, and K. Shih, Fabrication of Heterostructured g-C₃N₄/Ag-TiO₂ Hybrid Photocatalyst with Enhanced Performance in Photocatalytic Conversion of CO₂ Under Simulated Sunlight Irradiation. *Appl. Surf. Sci.*, 2017. 402:198-207.
 25. Zhou, S., Y. Liu, J. Li, Y. Wang, G. Jiang, Z. Zhao, D. Wang, A. Duan, J. Liu, and Y. Wei, Facile in situ synthesis of graphitic carbon nitride (g-C₃N₄)-N-TiO₂ heterojunction as an efficient photocatalyst for the selective photoreduction of CO₂ to CO. *Appl. Catal. B: Environ.*, 2014. 158-159:20-29.
 26. Adekoya, D.O., M. Tahir, and N.A.S. Amin, g-C₃N₄/(Cu/TiO₂) nanocomposite for enhanced photoreduction of CO₂ to CH₃OH and HCOOH under UV/visible light. *J. CO₂ Util.*, 2017. 18:261-274.
 27. Balcombe, P., N.P. Brandon, and A.D. Hawkes, Characterising the distribution of methane and carbon dioxide emissions from the natural gas supply chain. *J. Cleaner Prod.*, 2018. 172:2019-2032.
 28. Heo, J., B. Lee, and H. Lim, Techno-economic analysis for CO₂ reforming of a medium-grade landfill gas in a membrane reactor for H₂ production. *J. Cleaner Prod.*, 2018. 172:2585-2593.
 29. Xu, L., F. Wang, M. Chen, X. Fan, H. Yang, D. Nie, and L. Qi, Alkaline-promoted Co-Ni bimetal ordered mesoporous catalysts with enhanced coke-resistant performance toward CO₂ reforming of CH₄. *J. CO₂ Util.*, 2017. 18:1-14.
 30. Khoja, A.H., M. Tahir, and N.A.S. Amin, Dry reforming of methane using different dielectric materials and DBD plasma reactor configurations. *Energy Convers. Manage.*, 2017. 144:262-274.

31. Moral, A., I. Reyero, C. Alfaro, F. Bimbela, and L.M. Gandia, Syngas production by means of biogas catalytic partial oxidation and dry reforming using Rh-based catalysts. *Catal. Today*, 2018. 299:280-288.
32. Goscianska, J., R. Pietrzak, and J. Matos, Catalytic performance of ordered mesoporous carbons modified with lanthanides in dry methane reforming. *Catal. Today*, 2018. 301:204-216.
33. Dębek, R., M. Motak, M.E. Galvez, T. Grzybek, and P. Da Costa, Promotion effect of zirconia on Mg(Ni,Al)O mixed oxides derived from hydrotalcites in CO₂ methane reforming. *Appl. Catal., B: Environ.*, 2018. 223:36-46.
34. Stroud, T., T.J. Smith, E. Le Saché, J.L. Santos, M.A. Centeno, H. Arellano-Garcia, J.A. Odriozola, and T.R. Reina, Chemical CO₂ recycling via dry and bi reforming of methane using Ni-Sn/Al₂O₃ and Ni-Sn/CeO₂-Al₂O₃ catalysts. *Appl. Catal., B: Environ.*, 2018. 224:125-135.
35. Itkulova, S.S., Y.Y. Nurmakanov, S.K. Kussanova, and Y.A. Boleubayev, Production of a hydrogen-enriched syngas by combined CO₂-steam reforming of methane over Co-based catalysts supported on alumina modified with zirconia. *Catal Today*, 2018. 299:272-279.
36. Yang, E.H., Y.S. Noh, G.H. Hong, and D.J. Moon, Combined steam and CO₂ reforming of methane over La_{1-x}Sr_xNiO₃ perovskite oxides. *Catal. Today*, 2018. 299:242-250.
37. Yazdanpour, N. and S. Sharifnia, Photocatalytic conversion of greenhouse gases (CO₂ and CH₄) using copper phthalocyanine modified TiO₂. *Sol. Energy Mater. Sol. Cells*, 2013. 118:1-8.
38. Merajin, M.T., S. Sharifnia, S.N. Hosseini, and N. Yazdanpour, Photocatalytic conversion of greenhouse gases (CO₂ and CH₄) to high value products using TiO₂ nanoparticles supported on stainless steel webnet. *J. Taiwan Inst. Chem. Eng.*, 2013. 44(2):239-246.
39. Shi, D., Y. Feng, and S. Zhong, Photocatalytic conversion of CH₄ and CO₂ to oxygenated compounds over Cu/CdS-TiO₂/SiO₂ catalyst. *Catalysis Today*, 2004. 98(4):505-509.
40. Teramura, K., T. Tanaka, H. Ishikawa, Y. Kohno, and T. Funabiki, Photocatalytic Reduction of CO₂ to CO in the Presence of H₂ or CH₄ as a Reductant over MgO. *J. Phys. Chem. B*, 2004. 108:346-354.

41. Han, B., W. Wei, L. Chang, P. Cheng, and Y.H. Hu, Efficient Visible Light Photocatalytic CO₂ Reforming of CH₄. *ACS Catal.*, 2015. 6(2):494-497.
42. Ali, K.A., A.Z. Abdullah, and A.R. Mohamed, Visible light responsive TiO₂ nanoparticles modified using Ce and La for photocatalytic reduction of CO₂ : Effect of Ce dopant content. *Appl. Catal., A: Gen.*, 2017. 537:111-120.
43. Priyanka, K.P., V.R. Revathy, P. Rosmin, B. Thrivedu, K.M. Elsa, J. Nimmymol, K.M. Balakrishna, and T. Varghese, Influence of La doping on structural and optical properties of TiO₂ nanocrystals. *Mater. Charact.*, 2016. 113:144-151.
44. Yu, L., X. Yang, J. He, Y. He, and D. Wang, One-step hydrothermal method to prepare nitrogen and lanthanum co-doped TiO₂ nanocrystals with exposed {001} facets and study on their photocatalytic activities in visible light. *J. Alloys Compd.*, 2015. 637:308-314.
45. Liu, Y., S. Zhou, J.M. Li, Y.J. Wang, G.Y. Jiang, Z. Zhao, B. Liu, X.Q. Gong, A.J. Duan, J. Liu, Y.C. Wei, and L.Q. Zhang, Photocatalytic reduction of CO₂ with water vapor on surface La-modified TiO₂ nanoparticles with enhanced CH₄ selectivity. *Appl Catal B-Environ*, 2015. 168:125-131.
46. Lang, Q., Y. Chen, T. Huang, L. Yang, S. Zhong, L. Wu, J. Chen, and S. Bai, Graphene “bridge” in transferring hot electrons from plasmonic Ag nanocubes to TiO₂ nanosheets for enhanced visible light photocatalytic hydrogen evolution. *Appl. Catal., B: Environ.*, 2018. 220:182-190.
47. Jiang, Z., J. Pan, B. Wang, and C. Li, Two dimensional Z-scheme AgCl/Ag/CaTiO₃ nano-heterojunctions for photocatalytic hydrogen production enhancement. *Appl. Surf. Sci.*, 2018. 436:519-526.
48. Tahir, M. and N.A.S. Amin, Photo-induced CO₂ reduction by hydrogen for selective CO evolution in a dynamic monolith photoreactor loaded with Ag-modified TiO₂ nanocatalyst. *Int. J. Hydrogen Energy*, 2017. 42(23):15507-15522.
49. Tahir, M., B. Tahir, and N.A.S. Amin, Synergistic effect in plasmonic Au/Ag alloy NPs co-coated TiO₂ NWs toward visible-light enhanced CO₂ photoreduction to fuels. *Appl. Catal., B: Environ.*, 2017. 204:548-560.
50. Low, J., S. Qiu, D. Xu, C. Jiang, and B. Cheng, Direct evidence and enhancement of surface plasmon resonance effect on Ag-loaded TiO₂ nanotube arrays for photocatalytic CO₂ reduction. *Appl. Surf. Sci.*, 2018. 434:423-432.

51. Shao, K., Y. Wang, M. Iqbal, L. Lin, K. Wang, X. Zhang, M. He, and T. He, Modification of Ag nanoparticles on the surface of SrTiO₃ particles and resultant influence on photoreduction of CO₂. *Appl. Surf. Sci.*, 2018. 434:717-724.
52. Yoshida, T., N. Yamamoto, T. Mizutani, M. Yamamoto, S. Ogawa, S. Yagi, H. Nameki, and H. Yoshida, Synthesis of Ag nanoparticles prepared by a solution plasma method and application as a cocatalyst for photocatalytic reduction of carbon dioxide with water. *Catal. Today*, 2018. 303:320-326.
53. Gao, H., P. Zhang, J. Zhao, Y. Zhang, J. Hu, and G. Shao, Plasmon enhancement on photocatalytic hydrogen production over the Z-scheme photosynthetic heterojunction system. *Appl. Catal., B: Environ.*, 2017. 210:297-305.
54. Sun, Z., H. Wang, Z. Wu, and L. Wang, g-C₃N₄ based composite photocatalysts for photocatalytic CO₂ reduction. *Catalysis Today*, 2018. 300:160-172.
55. Sun, Z., H. Wang, Z. Wu, and L. Wang, g-C₃N₄ based composite photocatalysts for photocatalytic CO₂ reduction. *Catalysis Today*, 2017.
56. Wen, J., J. Xie, X. Chen, and X. Li, A review on g-C₃N₄-based photocatalysts. *Appl. Surf. Sci.*, 2017. 391:72-123.
57. Ong, W.-J., L.-L. Tan, S.-P. Chai, S.-T. Yong, and A.R. Mohamed, Surface charge modification via protonation of graphitic carbon nitride (g-C₃N₄) for electrostatic self-assembly construction of 2D/2D reduced graphene oxide (rGO)/g-C₃N₄ nanostructures toward enhanced photocatalytic reduction of carbon dioxide to methane. *Nano Energy*, 2015. 13:757-770.
58. Ong, W.J., L.L. Tan, S.P. Chai, and S.T. Yong, Heterojunction engineering of graphitic carbon nitride (g-C₃N₄) via Pt loading with improved daylight-induced photocatalytic reduction of carbon dioxide to methane. *Dalton transactions*, 2015. 44(3):1249-1257.
59. Li, M., L. Zhang, M. Wu, Y. Du, X. Fan, M. Wang, L. Zhang, Q. Kong, and J. Shi, Mesoporous CeO₂/g-C₃N₄ nanocomposites: Remarkably enhanced photocatalytic activity for CO₂ reduction by mutual component activations. *Nano Energy*, 2016. 19:145-155.
60. Qin, J. and H. Zeng, Photocatalysts fabricated by depositing plasmonic Ag nanoparticles on carbon quantum dots/graphitic carbon nitride for broad

- spectrum photocatalytic hydrogen generation. *Appl. Catal. B: Environ.*, 2017. 209:161-173.
61. Wang, J.C., H.C. Yao, Z.Y. Fan, L. Zhang, J.S. Wang, S.Q. Zang, and Z.J. Li, Indirect Z-Scheme BiOI/g-C₃N₄ Photocatalysts with Enhanced Photoreduction CO₂ Activity under Visible Light Irradiation. *ACS Appl. Mater. Interfaces*, 2016. 8(6):3765-3775.
 62. Zhou, S., Y. Liu, J. Li, Y. Wang, G. Jiang, Z. Zhao, D. Wang, A. Duan, J. Liu, and Y. Wei, Facile in situ synthesis of graphitic carbon nitride (g-C₃N₄)-N-TiO₂ heterojunction as an efficient photocatalyst for the selective photoreduction of CO₂ to CO. *Appl. Catal., B: Environ.*, 2014. 158–159:20-29.
 63. Bafaqeer, A., M. Tahir, and N.A.S. Amin, Well-designed ZnV₂O₆/g-C₃N₄ 2D/2D nanosheets heterojunction with faster charges separation via pCN as mediator towards enhanced photocatalytic reduction of CO₂ to fuels. *Appl. Catal., B: Environ.*, 2019. 242:312-326.
 64. Tang, J.-y., W.-g. Zhou, R.-t. Guo, C.-y. Huang, and W.-g. Pan, Enhancement of photocatalytic performance in CO₂ reduction over Mg/g-C₃N₄ catalysts under visible light irradiation. *Catal. Commun.*, 2018. 107:92-95.
 65. Ola, O., M. Maroto-Valer, D. Liu, S. Mackintosh, C.-W. Lee, and J.C.S. Wu, Performance comparison of CO₂ conversion in slurry and monolith photoreactors using Pd and Rh-TiO₂ catalyst under ultraviolet irradiation. *Appl. Catal., B: Environ.*, 2012. 126:172-179.
 66. Yuan, K., L. Yang, X. Du, and Y. Yang, Performance analysis of photocatalytic CO₂ reduction in optical fiber monolith reactor with multiple inverse lights. *Energy Convers. Manage.*, 2014. 81:98-105.
 67. Chen, R., X. Cheng, X. Zhu, Q. Liao, L. An, D.D. Ye, X.F. He, and Z.B. Wang, High-performance optofluidic membrane microreactor with a mesoporous CdS/TiO₂/SBA-15@carbon paper composite membrane for the CO₂ photoreduction. *Chem. Eng. J.*, 2017. 316:911-918.
 68. Wang, T., L. Yang, X. Du, and Y. Yang, Numerical investigation on CO₂ photocatalytic reduction in optical fiber monolith reactor. *Energy Convers. Manage.*, 2013. 65:299-307.
 69. Tahir, M. and N.S. Amin, Performance analysis of nanostructured NiO–In₂O₃/TiO₂ catalyst for CO₂ photoreduction with H₂ in a monolith photoreactor. *Chem. Eng. J.*, 2016. 285:635-649.

70. Indrakanti, V.P., H.H. Schobert, and J.D. Kubicki, Quantum Mechanical Modeling of CO₂ Interactions with Irradiated Stoichiometric and Oxygen-Deficient Anatase TiO₂ Surfaces: Implications for the Photocatalytic Reduction of CO₂. *Energy Fuels*, 2009. 23(10):5247-5256.
71. Olah, G.A., A. Goepfert, and G.K. Prakash, Chemical recycling of carbon dioxide to methanol and dimethyl ether: from greenhouse gas to renewable, environmentally carbon neutral fuels and synthetic hydrocarbons. *J. Org. Chem.*, 2009. 74(2):487-498.
72. Benson, E.E., C.P. Kubiak, A.J. Sathrum, and J.M. Smieja, Electrocatalytic and homogeneous approaches to conversion of CO₂ to liquid fuels. *Chem. Soc. Rev.*, 2009. 38(1):89-99.
73. Stewart, C. and M.-A. Hessami, A study of methods of carbon dioxide capture and sequestration—the sustainability of a photosynthetic bioreactor approach. *Energy Convers. Manage.*, 2005. 46(3):403-420.
74. Nozaki, T., A. Ağral, S. Yuzawa, J.G.E. Han Gardeniers, and K. Okazaki, A single step methane conversion into synthetic fuels using microplasma reactor. *Chem. Eng. J.*, 2011. 166(1):288-293.
75. Yap, D., J.-M. Tatibouët, and C. Batiot-Dupeyrat, Catalyst assisted by non-thermal plasma in dry reforming of methane at low temperature. *Catal. Today*, 2018. 299:263-271.
76. Tao, X., M. Bai, X. Li, H. Long, S. Shang, Y. Yin, and X. Dai, CH₄-CO₂ reforming by plasma – challenges and opportunities. *Prog. Energy Combust. Sci.*, 2011. 37(2):113-124.
77. Yang, E.-h., Y.S. Noh, G.H. Hong, and D.J. Moon, Combined steam and CO₂ reforming of methane over La_{1-x} Sr_xNiO₃ perovskite oxides. *Catal. Today*, 2018. 299:242-250.
78. Osazuwa, O.U. and C.K. Cheng, Catalytic conversion of methane and carbon dioxide (greenhouse gases) into syngas over samarium-cobalt-trioxides perovskite catalyst. *J. Cleaner Prod.*, 2017. 148:202-211.
79. Chein, R.-Y., C.-Y. Wang, and C.-T. Yu, Parametric study on catalytic tri-reforming of methane for syngas production. *Energy*, 2017. 118:1-17.
80. Itkulova, S.S., Y.Y. Nurmakanov, S.K. Kussanova, and Y.A. Boleubayev, Production of a hydrogen-enriched syngas by combined CO₂ -steam reforming

- of methane over Co-based catalysts supported on alumina modified with zirconia. *Catal. Today*, 2018. 299:272-279.
81. Li, X.K., Z.J. Zhuang, W. Li, and H.Q. Pan, Photocatalytic reduction of CO₂ over noble metal-loaded and nitrogen-doped mesoporous TiO₂. *Appl. Catal., A: Gen.*, 2012. 429:31-38.
 82. Zhao, Z., J. Fan, S. Liu, and Z. Wang, Optimal design and preparation of titania-supported CoPc using sol-gel for the photo-reduction of CO₂. *Chem. Eng. J.*, 2009. 151(1-3):134-140.
 83. Ohtani, B., Photocatalysis A to Z—What we know and what we do not know in a scientific sense. *J. Photochem. Photobiol., C*, 2010. 11(4):157-178.
 84. Yuliati, L., H. Itoh, and H. Yoshida, Photocatalytic conversion of methane and carbon dioxide over gallium oxide. *Chemical Physics Letters*, 2008. 452:178-182.
 85. Adekoya, D.O., M. Tahir, and N.A.S. Amin, g-C₃N₄/(Cu/TiO₂) nanocomposite for enhanced photoreduction of CO₂ to CH₃OH and HCOOH under UV/visible light. *Journal of CO₂ Utilization*, 2017. 18:261-274.
 86. Sun, Z., Haiqiang Wang, Z. Wu, L. Wang, Z. Sun, H. Wang, Z. Wu, and L. Wang, g-C₃N₄ based composite photocatalysts for photocatalytic CO₂ reduction. *Catal. Today*, 2018. 300:160-172.
 87. Yuliati, L., H. Itoh, and H. Yoshida, Photocatalytic conversion of methane and carbon dioxide over gallium oxide. *Chem. Phys. Lett.*, 2008. 452(1-3):178-182.
 88. László, B., K. Baán, E. Varga, A. Oszkó, A. Erdöhelyi, Z. Kónya, and J. Kiss, Photo-induced reactions in the CO₂-methane system on titanate nanotubes modified with Au and Rh nanoparticles. *Appl. Catal. B: Environ.*, 2016. 199:473-484.
 89. Chen, X., Y. Li, X. Pan, D. Cortie, X. Huang, and Z. Yi, Photocatalytic oxidation of methane over silver decorated zinc oxide nanocatalysts. *Nature communications*, 2016. 7:12273.
 90. Teramura, K., T. Tanaka, H. Ishikawa, Y. Kohno, and T. Funabiki, Photocatalytic Reduction of CO₂ to CO in the Presence of H₂ or CH₄ as a Reductant over MgO. *J. Phys. Chem. B*, 2004. 108(1):346-354.
 91. Zeng, C., T. Hu, N. Hou, S. Liu, W. Gao, R. Cong, and T. Yang, Photocatalytic pure water splitting activities for ZnGa₂O₄ synthesized by various methods. *Mater. Res. Bull.*, 2015. 61:481-485.

92. Inoue, T., F. Akira, K. Satoshi, and H. Kenichi, Photoelectrocatalytic reduction of carbon dioxide in aqueous suspensions of semiconductor powders. *Nature*, 1979. 277:637-638.
93. Wang, Z., K. Teramura, Z. Huang, S. Hosokawa, Y. Sakata, and T. Tanaka, Tuning the selectivity toward CO evolution in the photocatalytic conversion of CO₂ with H₂O through the modification of Ag-loaded Ga₂O₃ with a ZnGa₂O₄ layer. *Catal. Sci. Technol.*, 2016. 6(4):1025-1032.
94. Ola, O. and M.M. Maroto-Valer, Review of material design and reactor engineering on TiO₂ photocatalysis for CO₂ reduction. *J. Photochem. Photobiol C: Photochem. Rev.*, 2015. 24:16-42.
95. Tahir, M., B. Tahir, N.A.S. Amin, and Z.Y. Zakaria, Photo-induced reduction of CO₂ to CO with hydrogen over plasmonic Ag-NPs/TiO₂ NWs core/shell hetero-junction under UV and visible light. *J. CO₂ Util.*, 2017. 18:250-260.
96. Xiong, Z., Z. Lei, S. Ma, X. Chen, B. Gong, Y. Zhao, J. Zhang, C. Zheng, and J.C.S. Wu, Photocatalytic CO₂ reduction over V and W codoped TiO₂ catalyst in an internal-illuminated honeycomb photoreactor under simulated sunlight irradiation. *Appl. Catal., B: Environ.*, 2017. 219:412-424.
97. Zhang, Q., T. Gao, J.M. Andino, and Y. Li, Copper and iodine co-modified TiO₂ nanoparticles for improved activity of CO₂ photoreduction with water vapor. *Appl. Catal., B: Environ.*, 2012. 123-124:257-264.
98. Tan, J.Z.Y., Y. Fernández, D. Liu, M. Maroto-Valer, J. Bian, and X. Zhang, Photoreduction of CO₂ using copper-decorated TiO₂ nanorod films with localized surface plasmon behavior. *Chem. Phys. Lett.*, 2012. 531:149-154.
99. Truong, Q.D., J.-Y. Liu, C.-C. Chung, and Y.-C. Ling, Photocatalytic reduction of CO₂ on FeTiO₃/TiO₂ photocatalyst. *Catal. Commun.*, 2012. 19:85-89.
100. Tong, Y., L. Chen, S. Ning, N. Tong, Z. Zhang, H. Lin, F. Li, and X. Wang, Photocatalytic reduction of CO₂ to CO over the Ti-Highly dispersed HZSM-5 zeolite containing Fe. *Appl. Catal., B: Environ.*, 2017. 203:725-730.
101. Xu, F., J. Zhang, B. Zhu, J. Yu, and J. Xu, CuInS₂ sensitized TiO₂ hybrid nanofibers for improved photocatalytic CO₂ reduction. *Appl. Catal., B: Environ.*, 2018. 230:194-202.
102. Song, H., R. Wu, Y. Liang, H. Xiong, and G. Ji, Facile synthesis of 3D nanoplate-built CdWO₄/BiOI heterostructures with highly enhanced

- photocatalytic performance under visible-light irradiation. *Colloids Surf., A*, 2017. 522:346-354.
103. Wu, M., M. Zhang, T. Lv, M. Guo, J. Li, C.A. Okonkwo, Q. Liu, and L. Jia, The effect of calcination atmosphere upon the photocatalytic performance of Au-La₂O₃/TiO₂ for hydrogen production from formic acid. *Appl. Catal., A: Gen.*, 2017. 547:96-104.
 104. Xiong, Z., Z. Lei, Z. Xu, X. Chen, B. Gong, Y. Zhao, H. Zhao, J. Zhang, and C. Zheng, Flame spray pyrolysis synthesized ZnO/CeO₂ nanocomposites for enhanced CO₂ photocatalytic reduction under UV–Vis light irradiation. *J. CO₂ Util.*, 2017. 18:53-61.
 105. Zhang, H., S. Ni, Y. Mi, and X. Xu, Ruddlesden-Popper compound Sr₂TiO₄ co-doped with La and Fe for efficient photocatalytic hydrogen production. *J. Catal.*, 2018. 359:112-121.
 106. Wang, R., S. Ni, G. Liu, and X. Xu, Hollow CaTiO₃ cubes modified by La/Cr co-doping for efficient photocatalytic hydrogen production. *Appl. Catal., B: Environ.*, 2018. 225:139-147.
 107. Kumar, P., C. Joshi, A. Barras, B. Sieber, A. Addad, L. Boussekey, S. Szunerits, R. Boukherroub, and S.L. Jain, Core–shell structured reduced graphene oxide wrapped magnetically separable rGO@CuZnO@Fe₃O₄ microspheres as superior photocatalyst for CO₂ reduction under visible light. *Appl. Catal., B: Environ.*, 2017. 205:654-665.
 108. Pham, T.-D. and B.-K. Lee, Novel capture and photocatalytic conversion of CO₂ into solar fuels by metals co-doped TiO₂ deposited on PU under visible light. *Appl. Catal., A: Gen.*, 2017. 529:40-48.
 109. Tahir, M. and N.S. Amin, Indium-doped TiO₂ nanoparticles for photocatalytic CO₂ reduction with H₂O vapors to CH₄. *Appl. Catal., B: Environ.*, 2015. 162:98-109.
 110. Wang, Z., K. Teramura, S. Hosokawa, and T. Tanaka, Photocatalytic conversion of CO₂ in water over Ag-modified La₂Ti₂O₇. *Appl. Catal., B: Environ.*, 2015. 163:241-247.
 111. Rani, S., N. Bao, and S.C. Roy, Solar Spectrum Photocatalytic Conversion of CO₂ and Water Vapor Into Hydrocarbons Using TiO₂ Nanoparticle Membranes. *Appl. Surf. Sci.*, 2014. 289:203-208.

112. Tang, C., W. Hou, E. Liu, X. Hu, and J. Fan, CeF₃/TiO₂ composite as a novel visible-light-driven photocatalyst based on upconversion emission and its application for photocatalytic reduction of CO₂. *J. Lumin.*, 2014. 154:305-309.
113. Ohno, T., N. Murakami, T. Koyanagi, and Y. Yang, Photocatalytic reduction of CO₂ over a hybrid photocatalyst composed of WO₃ and graphitic carbon nitride (g-C₃N₄) under visible light. *J. CO₂ Util.*, 2014. 6:17-25.
114. Lin, J., Z. Pan, and X. Wang, Photochemical Reduction of CO₂ by Graphitic Carbon Nitride Polymers. *ACS Sustainable Chem. Eng.*, 2014. 2(3):353-358.
115. Cao, S.W., X.F. Liu, Y.P. Yuan, Z.Y. Zhang, Y.S. Liao, J. Fang, S.C.J. Loo, T.C. Sum, and C. Xue, Solar-to-fuels conversion over In₂O₃/g-C₃N₄ hybrid photocatalysts. *Appl. Catal. B*, 2014. 147:940-946.
116. Yang, Z.X., J.F. Xu, C.X. Wu, H. Jing, P.Q. Li, and H.Z. Yin, New insight into photoelectric converting CO₂ to CH₃OH on the one-dimensional ribbon CoPc enhanced Fe₂O₃ NTs. *Appl. Catal. B*, 2014. 156:249-256.
117. Yu, J., K. Wang, W. Xiao, and B. Cheng, Photocatalytic reduction of CO₂ into hydrocarbon solar fuels over g-C₃N₄-Pt nanocomposite photocatalysts. *Phys Chem Chem Phys*, 2014. 16(23):11492-11501.
118. Li, Q., L. Zong, C. Li, and J. Yang, Photocatalytic reduction of CO₂ on MgO/TiO₂ nanotube films. *Appl. Surf. Sci.*, 2014. 314:458-463.
119. Mei, B., A. Pougin, and J. Strunk, Influence of photodeposited gold nanoparticles on the photocatalytic activity of titanate species in the reduction of CO₂ to hydrocarbons. *J. Catal.*, 2013. 306:184-189.
120. Feng, X., J.D. Sloppy, T.J. LaTempa, M. Paulose, S. Komarneni, N. Bao, and C.A. Grimes, Synthesis and deposition of ultrafine Pt nanoparticles within high aspect ratio TiO₂ nanotube arrays: application to the photocatalytic reduction of carbon dioxide. *J. Mater. Chem.*, 2011. 21(35):13429.
121. Tahir, M. and N.S. Amin, Photocatalytic reduction of carbon dioxide with water vapors over montmorillonite modified TiO₂ nanocomposites. *Appl. Catal., B: Environ.*, 2013. 142-143:512-522.
122. Krejčíková, S., L. Matějová, K. Kočí, L. Obalová, Z. Matěj, L. Čapek, and O. Šolcová, Preparation and characterization of Ag-doped crystalline titania for photocatalysis applications. *Appl. Catal., B*, 2012. 111-112:119-125.
123. Kočí, K., K. Matěj, L. Obalová, S. Krejčíková, Z. Lacný, D. Plachá, L. Čapek, A. Hospodková, and O. Šolcová, Effect of silver doping on the TiO₂ for

- photocatalytic reduction of CO₂. *Appl. Catal., B: Environ.*, 2010. 96(3-4):239-244.
124. Zhang, H. and A. Yu, Photophysics and Photocatalysis of Carbon Nitride Synthesized at Different Temperatures. *J. Phys. Chem. C*, 2014. 118(22):11628-11635.
125. Zhu, J., P. Xiao, H. Li, and S.A. Carabineiro, Graphitic carbon nitride: synthesis, properties, and applications in catalysis. *ACS Appl. Mater. Interfaces*, 2014. 6(19):16449-16465.
126. Muñoz-Batista, M.J., M. Fernández-García, and A. Kubacka, Promotion of CeO₂-TiO₂ photoactivity by g-C₃N₄: Ultraviolet and visible light elimination of toluene. *Appl. Catal., B*, 2015. 164:261-270.
127. Ye, J., Y. Wang, Y. Liu, and H. Wang, Steam reforming of ethanol over Ni/Ce_xTi_{1-x}O₂ catalysts. *Int J Hydrogen Energy*, 2008. 33(22):6602-6611.
128. Yin, G., M. Nishikawa, Y. Nosaka, N. Srinivasan, D. Atarashi, E. Sakai, and M. Miyauchi, Photocatalytic Carbon Dioxide Reduction by Copper Oxide Nanocluster-Grafted Niobate Nanosheets. *ACS Nano*, 2015. 9(2):2111-2119.
129. Zhang, Q., S. Liu, Y. Zhang, A. Zhu, J. Li, and X. Du, Enhancement of the photocatalytic activity of g-C₃N₄ via treatment in dilute NaOH aqueous solution. *Mater. Lett.*, 2016. 171:79-82.
130. Lin, B., C. Xue, X. Yan, G. Yang, G. Yang, and B. Yang, Facile fabrication of novel SiO₂/g-C₃N₄ core-shell nanosphere photocatalysts with enhanced visible light activity. *Appl. Surf. Sci.*, 2015. 357, Part A:346-355.
131. Ong, W.J., L.L. Tan, Y.H. Ng, S.T. Yong, and S.P. Chai, Graphitic Carbon Nitride (g-C₃N₄)-Based Photocatalysts for Artificial Photosynthesis and Environmental Remediation: Are We a Step Closer To Achieving Sustainability? *Chem. Rev.*, 2016. 116(12):7159-7329.
132. Chen, X.-J., G. Cabello, D.-Y. Wu, and Z.-Q. Tian, Surface-enhanced Raman spectroscopy toward application in plasmonic photocatalysis on metal nanostructures. *J. Photochem. Photobiol., C*, 2014. 21:54-80.
133. Sellappan, R., M.G. Nielsen, F. González-Posada, P.C.K. Vesborg, I. Chorkendorff, and D. Chakarov, Effects of plasmon excitation on photocatalytic activity of Ag/TiO₂ and Au/TiO₂ nanocomposites. *J. Catal.*, 2013. 307:214-221.

134. Hou, W., W.H. Hung, P. Pavaskar, A. Goepfert, M. Aykol, and S.B. Cronin, Photocatalytic Conversion of CO₂ to Hydrocarbon Fuels via Plasmon-Enhanced Absorption and Metallic Interband Transitions. *ACS Catal.*, 2011. 1(8):929-936.
135. Zhang, W., L. Zhou, and H. Deng, Ag modified g-C₃N₄ composites with enhanced visible-light photocatalytic activity for diclofenac degradation. *J. Mol. Catal. A: Chem.*, 2016. 423:270-276.
136. Ding, L.L., J.P. Ge, W.Q. Zhou, J.P. Gao, Z.Y. Zhang, and Y. Xiong, Nanogold-functionalized g-C₃N₄ nanohybrids for sensitive impedimetric immunoassay of prostate-specific antigen using enzymatic biocatalytic precipitation. *Biosens. Bioelectron.*, 2016. 85:212-219.
137. Jiang, J., J. Yu, and S. Cao, Au/PtO nanoparticle-modified g-C₃N₄ for plasmon-enhanced photocatalytic hydrogen evolution under visible light. *J. Colloid Interface Sci.*, 2016. 461:56-63.
138. Ramesh Reddy, N., M. Mamatha Kumari, K.K. Cheralathan, and M.V. Shankar, Enhanced photocatalytic hydrogen production activity of noble metal free MWCNT-TiO₂ nanocomposites. *Int J Hydrogen Energy*, 2018. 43(8):4036-4043.
139. Humayun, M., Q. Fua, Z. Zheng, H. Li, and W. Luo, Improved visible-light catalytic activities of novel Au/P-doped g-C₃N₄ photocatalyst for solar fuel production and mechanism. *Appl. Catal., A: Gen.*, 2018. 568:139-147.
140. Tahir, B., M. Tahir, and N.A.S. Amin, Photo-induced CO₂ reduction by CH₄/H₂O to fuels over Cu-modified g-C₃N₄ nanorods under simulated solar energy. *Appl. Surf. Sci.*, 2017. 419:875-885.
141. Kočí, K., M. Reli, O. Kozák, Z. Lacný, D. Plachá, P. Praus, and L. Obalová, Influence of reactor geometry on the yield of CO₂ photocatalytic reduction. *Catal. Today*, 2011. 176(1):212-214.
142. Tang, J.-y., R.-t. Guo, W.-g. Pan, W.-g. Zhou, and C.-y. Huang, Visible light activated photocatalytic behaviour of Eu (III) modified g-C₃N₄ for CO₂ reduction and H₂ evolution. *Appl. Surf. Sci.*, 2019. 467-468:206-212.
143. Shi, G., L. Yang, Z. Liu, X. Chen, J. Zhou, and Y. Yu, Photocatalytic reduction of CO₂ to CO over copper decorated g-C₃N₄ nanosheets with enhanced yield and selectivity. *Appl. Surf. Sci.*, 2018. 427:1165-1173.

144. Cao, S., Y. Li, B. Zhu, M. Jaroniec, and J. Yua, Facet effect of Pd cocatalyst on photocatalytic CO₂ reduction over g-C₃N₄. *J. Catal.*, 2017. 349:208-217.
145. Mulewa, W., M. Tahir, and N.A.S. Amin, MMT-supported Ni/TiO₂ nanocomposite for low temperature ethanol steam reforming toward hydrogen production. *Chem. Eng. J.*, 2017. 326:956-969.
146. Bai, Y., T. Chen, P. Wang, L. Wang, L. Ye, X. Shi, and W. Bai, Size-dependent role of gold in g-C₃N₄/BiOBr/Au system for photocatalytic CO₂ reduction and dye degradation. *Sol. Energy Mater. Sol. Cells*, 2016. 157:406-414.
147. Di, T., B. Zhu, B. Cheng, J. Yu, and J. Xu, A direct Z-scheme g-C₃N₄/SnS₂ photocatalyst with superior visible-light CO₂ reduction performance. *J. Catal.*, 2017. 352:532-541.
148. Truc, N.T.T., Nguyen Thi Hanhb, M.V. Nguyen, N.T.P.L. Chid, N.V. Noi, D.T. Tran, M.N. Ha, D.Q. Trung, and T.-D. Pham, Novel direct Z-scheme Cu₂V₂O₇/g-C₃N₄ for visible light photocatalytic conversion of CO₂ into valuable fuels. *Appl Surf Sci*, 2018. 457:968-974.
149. Murugesan, P., S. Narayanan, M. Manickam, P.K. Murugesan, and R. Subbiah, A direct Z-scheme plasmonic AgCl@g-C₃N₄ heterojunction photocatalyst with superior visible light CO₂ reduction in aqueous medium. *Appl Surf Sci*, 2018. 450:516-526.
150. Rather, R.A., M. Khan, and I.M.C. Lo, High charge transfer response of g-C₃N₄/Ag/AgCl/BiVO₄ microstructure for the selective photocatalytic reduction of CO₂ to CH₄ under alkali activation. *J. Catal.*, 2018. 366:28-36.
151. Li, J., M. Zhang, Q. Li, and J. Yang, Enhanced visible light activity on direct contact Z-scheme g-C₃N₄-TiO₂ photocatalyst. *Appl. Surf. Sci.*, 2017. 391:184-193.
152. Sun, B., N. Lu, Y. Su, H. Yu, X. Meng, and Z. Gao, Decoration of TiO₂ nanotube arrays by graphitic-C₃N₄ quantum dots with improved photoelectrocatalytic performance. *Appl. Surf. Sci.*, 2017. 394:479-487.
153. Zhang, Y., Q. Wang, J. Lu, Q. Wang, and Y. Cong, Synergistic photoelectrochemical reduction of Cr(VI) and oxidation of organic pollutants by g-C₃N₄/TiO₂-NTs electrodes. *Chemosphere*, 2016. 162:55-63.

154. Tang, D. and G. Zhang, Fabrication of AgFeO₂/g-C₃N₄ nanocatalyst with enhanced and stable photocatalytic performance. *Appl. Surf. Sci.*, 2017. 391:415-422.
155. Lu, Y., X. Zhang, Y. Chu, H. Yu, M. Huo, J. Qu, J.C. Crittenden, H. Huo, and X. Yuan, Cu₂O nanocrystals/TiO₂ microspheres film on a rotating disk containing long-afterglow phosphor for enhanced round-the-clock photocatalysis. *Appl. Catal., B: Environ.*, 2018. 224:239-248.
156. Difa Xua, Bei Cheng, Weikang Wang, Chuanjia Jiang, and J. Yu, Ag₂CrO₄/g-C₃N₄/graphene oxide ternary nanocomposite Z-scheme photocatalyst with enhanced CO₂ reduction activity. *Appl. Catal., B: Environ.*, 2018. 231:368-380.
157. Xu, D., B. Cheng, W. Wang, C. Jiang, and J. Yu, Ag₂CrO₄/g-C₃N₄ /graphene oxide ternary nanocomposite Z-scheme photocatalyst with enhanced CO₂ reduction activity. *Appl. Catal., B: Environ.*, 2018. 242:139-147.
158. Nie, N., L. Zhang, J. Fu, B. Cheng, and J. Yu, Self-assembled hierarchical direct Z-scheme g-C₃N₄/ZnO microspheres with enhanced photocatalytic CO₂ reduction performance. *Appl. Surf. Sci.*, 2018. 441:12-22.
159. Liu, H., Z. Zhang, J. Meng, and J. Zhang, Novel visible-light-driven CdIn₂S₄/mesoporous g-C₃N₄ hybrids for efficient photocatalytic reduction of CO₂ to methanol. *J. Mol. Catal.*, 2017. 430:9-19.
160. Ahmad Beigi, A., S. Fatemi, and Z. Salehi, Synthesis of nanocomposite CdS/TiO₂ and investigation of its photocatalytic activity for CO₂ reduction to CO and CH₄ under visible light irradiation. *J. CO₂ Util.*, 2014. 7:23-29.
161. Adekoya, D.O., M. Tahir, and N.A.S. Amin, g-C₃N₄/(Cu/TiO₂) nanocomposite for enhanced photoreduction of CO₂ to CH₃ OH and HCOOH under UV/visible light. *J. CO₂ Util.*, 2017. 18:261-274.
162. Li, M., L. Zhang, M. Wu, Y. Du, X. Fan, M. Wang, L. Zhang, Q. Kong, and J. Shin, Mesostructured CeO₂/g-C₃N₄ nanocomposites: Remarkably enhanced photocatalytic activity for CO₂ reduction by mutual component activations. *Nano Energy*, 2016. 19:145-155.
163. Lasa, H.d., B. Serrano, and M. Salices, *Photocatalytic Reaction Engineering*. 2005, New York: Springer.

164. G.R. Dey, A.D. Belapurkar, and K. Kishore, Photo-catalytic reduction of carbon dioxide to methane using TiO₂ as suspension in water. *J. Photochem. Photobiol. A: Chem.*, 2004. 163:503–508.
165. Dey, G.R., Chemical Reduction of CO₂ to Different Products during Photo Catalytic Reaction on TiO₂ under Diverse Conditions: an Overview. *J. Nat. Gas Chem.*, 2007. 16:217-226.
166. Wu, J., H. Lin, and C. Lai, Photo reduction of CO₂ to methanol using optical-fiber photoreactor. *Appl. Catal., A: Gen.*, 2005. 296(2):194-200.
167. Galinska, A. and J. Walendziewski, Photocatalytic Water Splitting over Pt-TiO₂ in the Presence of Sacrificial Reagents. *Energy Fuels*, 2005. 19(3):1143-1147.
168. Adachi, K., K. Ohta, and T. Mizuno, Photocatalytic Reduction of Carbon dioxide To Hydrocarbons Using Copper Loaded Titanium Dioxide *Sol. Energy Mater. Sol. Cells*, 1994. 53(2):187-190.
169. Lo, C.C., C.H. Hung, C.S. Yuan, and Y.L. Hung, Parameter effects and reaction pathways of photoreduction of CO₂ over TiO₂/SO₄²⁻ photocatalyst. *Chin. J. Catal.*, 2007. 28(6):528-534.
170. Lo, C.-C., C.-H. Hung, C.-S. Yuan, and J.-F. Wu, Photoreduction of carbon dioxide with H₂ and H₂O over TiO₂ and ZrO₂ in a circulated photocatalytic reactor. *Sol. Energy Mater. Sol. Cells*, 2007. 91:1765–1774.
171. Halmann, M., M. Ulman, and B.A. Blajeni, Photochemical SolarCollector for the Photoassisted Reduction of Aqueous Carbon Dioxide. *Sol. Energy*, 1983. 31:429–431.
172. M. Halmann and V. Katzir, Photoassisted Carbon Dioxide Reduction On Aqueous Suspensions of Titanium Dioxide. *Sol. Energy Mater.*, 1984. 10:85-91.
173. Shi, D., Y. Feng, and S. Zhong, Photocatalytic conversion of CH₄ and CO₂ to oxygenated compounds over Cu/CdS–TiO₂/SiO₂ catalyst. *Catal. Today*, 2004. 98:505–509.
174. Wang, C., R.L. Thompson, J. Baltrus, and C. Matranga, Visible Light Photoreduction of CO₂ Using CdSe/Pt/TiO₂ Heterostructured Catalysts. *J. Phys. Chem. Lett.*, 2010. 1:48–53.

175. Imoberdorf, G.E., A.E. Cassano, H.A. Irazoqui, and O.M. Alfano, Optimal design and modeling of annular photocatalytic wall reactors. *Catal. Today*, 2007. 129(1-2):118-126.
176. Ling, C.M., A.R. Mohamed, and S. Bhatia, Performance of photocatalytic reactors using immobilized TiO₂ film for the degradation of phenol and methylene blue dye present in water stream. *Chemosphere*, 2004. 57(7):547-554.
177. Tomašić, V., F. Jović, and Z. Gomzi, Photocatalytic oxidation of toluene in the gas phase: Modelling an annular photocatalytic reactor. *Catal. Today*, 2008. 137(2-4):350-356.
178. Vincent, G., P.M. Marquaire, and O. Zahraa, Abatement of volatile organic compounds using an annular photocatalytic reactor: Study of gaseous acetone. *J. Photochem. Photobiol., A*, 2008. 197(2-3):177-189.
179. Du, P., J.T. Cameiro, J.A. Moulijn, and G. Mul, A novel photocatalytic monolith reactor for multiphase heterogeneous photocatalysis. *Appl. Catal., A*, 2008. 334(1-2):119-128.
180. Tahir, M. and N.S. Amin, Recycling of carbon dioxide to renewable fuels by photocatalysis: Prospects and challenges. *Renewable Sustainable Energy Rev.*, 2013. 25:560-579.
181. Wu, J.C.S., H.M. Lin, and C.L. Lai, Photoreduction of CO₂ to methanol using optical-fiber photoreactor. *Appl. Catal., A*, 2005. 296(2):194-200.
182. Liou, P.-Y., S.-C. Chen, J.C.S. Wu, D. Liu, S. Mackintosh, M. Maroto-Valer, and R. Linforth, Photocatalytic CO₂ reduction using an internally illuminated monolith photoreactor. *Energy Environ. Sci.*, 2011. 4(4):1487.
183. Guizard, C. and A. Princivalle, Preparation and characterization of catalyst thin films. *Catal. Today*, 2009. 146(3-4):367-377.
184. Joo, H. and J.-h. Lee, Polyaniline nanofiber coated monolith reactor for enzymatic bioconversion. *J. Mol. Catal. B: Enzym.*, 2010. 67(3-4):179-183.
185. Harriott, P., *Chemical Reactor Design*. 2003, Cornell University Ithaca, New York, U.S.A: Marcel Dekker, Inc.
186. Perry, R.H. and D. Green, *Chemical Engineers' Handbook*,. 6 ed. 1984, New York.: McGraw-Hill.

187. Chen, J., H. Yang, N. Wang, Z. Ring, and T. Dabros, Mathematical modeling of monolith catalysts and reactors for gas phase reactions. *Appl. Catal. A: Gen.*, 2008. 345(1):1-11.
188. Du, P., J.T. Carneiro, Jacob A. Moulijn, and Guido Mul, A novel photocatalytic monolith reactor for multiphase heterogeneous photocatalysis. *Appl. Catal., A: Gen.*, 2008(334):119–128.
189. Carneiro, J.T., C.-C. Yang, J.A. Moulijn, and G. Mul, The effect of water on the performance of TiO₂ in photocatalytic selective alkane oxidation. *J. Catal.*, 2011. 277:129-133.
190. Gonzalez, C.A., A.N. Ardila, M.d. Correa, M.A. Martinez, and G. Fuentes-Zurit, Pd/TiO₂ Washcoated Cordierite Minimonoliths for Hydrodechlorination of Light Organochlorinated Compounds. *Ind. Eng. Chem. Res.*, 2007. 46:7961-7969.
191. Joo, H. and J.-h. Lee, Polyaniline nanofiber coated monolith reactor for enzymatic bioconversion. *J. Mol. Catal. B: Enzym.*, 2010. 67:179-183.
192. Chen, J., H. Yang, N. Wang, Z. Ring, and T. Dabros, Mathematical modeling of monolith catalysts and reactors for gas phase reactions. *Appl. Catal., A: Gen.*, 2008. 345:1-11.
193. Yang, Y., W. Guo, Y. Guo, Y. Zhao, and X. Yuan, Fabrication of Z-scheme plasmonic photocatalyst Ag@AgBr/g-C₃N₄ with enhanced visible-light photocatalytic activity. *J. Hazard. Mater.*, 2014. 271:150-159.
194. Liu, H., J. Zhao, C. Li, and S. Ji, Conceptual design and CFD simulation of a novel metal-based monolith reactor with enhanced mass transfer. *Catal. Today*, 2005. 105(3-4):401-406.
195. Phairat, U., M. Dena, V. Amornvadee, and T. Paitoon, Photocatalytic Process for CO₂ Emission Reduction from Industrial Flue Gas Streams. *Ind. Eng. Chem. Res.*, 2006. 45(8):2558-2568.
196. Huang, X., Y. Meng, P. Liang, and Y. Qian, Operational conditions of a membrane filtration reactor coupled with photocatalytic oxidation. *Sep. Purif. Technol.*, 2007. 55(2):165-172.
197. McCullagh, C., P.K.J. Robertson, M. Adams, P.M. Pollard, and A. Mohammed, Development of a slurry continuous flow reactor for photocatalytic treatment of industrial waste water. *J. Photochem. Photobiol., A*, 2010. 211(1):42-46.

198. Tahir, M. and N.S. Amin, Advances in visible light responsive titanium oxide-based photocatalysts for CO₂ conversion to hydrocarbon fuels. *Energy Convers. Manage.*, 2013. 76:194-214.
199. Ola, O. and M.M. Maroto-Valer, Copper based TiO₂ honeycomb monoliths for CO₂ photoreduction. *Catal. Sci. Technol*, 2014. 4(6):1631-1637.
200. Tahir, M. and N.S. Amin, Photocatalytic CO₂ reduction and kinetic study over In/TiO₂ nanoparticles supported microchannel monolith photoreactor. *Appl. Catal. A*, 2013. 467:483-496.
201. Chen, D., F. Li, and A.K. Ray, Effect of mass transfer and catalyst layer thickness on photocatalytic reaction. *AIChE J*, 2000. 46(5):1034-1045.
202. Van Gerven, T., G. Mul, J. Moulijn, and A. Stankiewicz, A review of intensification of photocatalytic processes. *Chem. Eng. Process*, 2007. 46(9):781-789.
203. Dijkstra, M., A. Michorius, H. Buwalda, H. Panneman, J. Winkelman, and A. Beenackers, Comparison of the efficiency of immobilized and suspended systems in photocatalytic degradation. *Catal. Today*, 2001. 66(2-4):487-494.
204. Tan, S.S., L. Zou, and E. Hu, Kinetic modelling for photosynthesis of hydrogen and methane through catalytic reduction of carbon dioxide with water vapour. *Catal. Today*, 2008. 131(1-4):125-129.
205. Tahir, M. and N.S. Amin, Photocatalytic CO₂ reduction and kinetic study over In/TiO₂ nanoparticles supported microchannel monolith photoreactor. *Appl. Catal. A: Gen.*, 2013. 467:483-496.
206. Koci, K., L. Obalova, L. Matejova, D. Placha, Z. Lacny, J. Jirkovsky, and O. Solcov, Effect of TiO₂ particle size on the photocatalytic reduction of CO₂. *Appl. Catal., B*, 2009. 89:494-502.
207. Morris, A.J., G.J. Meyer, and E. Fujita, Molecular approaches to the photocatalytic reduction of carbon dioxide for solar fuels. *Acc. Chem. Res.*, 2009. 42(12):1983-1994.
208. Tan, L.-L., W.-J. Ong, S.-P. Chai, and A.R. Mohamed, Photocatalytic reduction of CO₂ with H₂O over graphene oxide-supported oxygen-rich TiO₂ hybrid photocatalyst under visible light irradiation: Process and kinetic studies. *Chem. Eng. J.*, 2017. 308:248-255.
209. Koci, K., L. Obalova, and O. Solcova, Kinetic Study of Photocatalytic Reduction of CO₂ Over TiO₂. *Chem. Process Engin.*, 2010. 31:395-407.

210. Tahir, M. and N.S. Amin, Photocatalytic CO₂ reduction with H₂O vapors using montmorillonite/TiO₂ supported microchannel monolith photoreactor. *Chem. Eng. J.*, 2013. 230:314-327.
211. Chong, S., S. Wang, M. Tade, A. H. Ming, and V. Pareek, Simulations of Photodegradation of Toluene and Formaldehyde in a Monolith Reactor Using Computational Fluid Dynamics. *Amer. Instit. Chem. Engin.*, 2011. 57(3):724-734.
212. Tahir, B., M. Tahir, and N.S. Amin, Gold–indium modified TiO₂ nanocatalysts for photocatalytic CO₂ reduction with H₂ as reductant in a monolith photoreactor. *Appl. Surf. Sci.*, 2015. 338:1-14.
213. Praus, P., O. Kozak, K. Koci, A. Panacek, and R. Dvorsky, CdS nanoparticles deposited on montmorillonite: preparation, characterization and application for photoreduction of carbon dioxide. *Int. J. Nanosci.*, 2011. 360(2):574-579.
214. Ho, C.-C., F. Kang, G.-M. Chang, S.-J. You, and Y.-F. Wang, Application of recycled lanthanum-doped TiO₂ immobilized on commercial air filter for visible-light photocatalytic degradation of acetone and NO. *Appl. Surf. Sci.*, 2019. 465:31-40.
215. Ellselami, L., H. Lachheb, and A. Houas, Synthesis, characterization and photocatalytic activity of Li-, Cd-, and La-doped TiO₂. *Mater. Sci. Semicond. Process.*, 2015. 36:103-114.
216. Dal'Toé, A.T.O., G.L. Colpani, N. Padoin, M.A. Fiori, and C. Soares, Lanthanum doped titania decorated with silver plasmonic nanoparticles with enhanced photocatalytic activity under UV-visible light. *Appl. Surf. Sci.*, 2018. 441:1057-1071.
217. Chaudhary, D., V.D. Vankar, and N. Khare, Noble metal-free g-C₃N₄/TiO₂ /CNT ternary nanocomposite with enhanced photocatalytic performance under visible-light irradiation via multi-step charge transfer process. *Solar Energy*, 2017. 158:132-139.
218. Jin, J., Q. Liang, C. Ding, Z. Li, and S. Xu, Simultaneous synthesis-immobilization of Ag nanoparticles functionalized 2D g-C₃N₄ nanosheets with improved photocatalytic activity. *J. Alloys Compd.*, 2017. 691:763-771.
219. Muniandy, L., F. Adam, A.R. Mohamed, A. Iqbal, and N.R.A. Rahman, Cu²⁺ coordinated graphitic carbon nitride (Cu-g-C₃N₄) nanosheets from melamine

- for the liquid phase hydroxylation of benzene and VOCs. *Appl. Surf. Sci.*, 2017. 398:43-55.
220. Qian, L., Y. Hou, Z. Yu, M. Li, F. Li, L. Sun, W. Luo, and G. Pan, Metal-induced Z-scheme CdS/Ag/g-C₃N₄ photocatalyst for enhanced hydrogen evolution under visible light: The synergy of MIP effect and electron mediator of Ag. *Molecular Catalysis*, 2018. 458:43-51.
 221. Tan, Y., Z. Shu, J. Zhou, T. Li, W. Wang, and Z. Zhao, One-step synthesis of nanostructured g-C₃N₄/TiO₂ composite for highly enhanced visible-light photocatalytic H₂ evolution. *Appl. Catal., B: Environ.*, 2018. 230:260-268.
 222. Zhao, H., Z.Y. Hu, J. Liu, Y. Li, M. Wu, G. Van Tendeloo, and B.L. Su, Blue-edge slow photons promoting visible-light hydrogen production on gradient ternary 3DOM TiO₂-Au-CdS photonic crystals. *Nano Energy*, 2018. 47:266-274.
 223. Zhou, X., Y. Chen, C. Li, L. Zhang, X. Zhang, X. Ning, L. Zhan, and J. Luo, Construction of LaNiO₃ nanoparticles modified g-C₃N₄ nanosheets for enhancing visible light photocatalytic activity towards tetracycline degradation. *Separation and Purification Technology*, 2019. 211:179-188.
 224. Ojha, D.P., H.P. Karki, and H.J. Kim, Design of ternary hybrid ATO/g-C₃N₄/TiO₂ nanocomposite for visible-light-driven photocatalysis. *J. Ind. Eng. Chem.*, 2018. 61:87-96.
 225. Kong, L., X. Zhang, C. Wang, J. Xu, X. Du, and L. Li, Ti³⁺ defect mediated g-C₃N₄/TiO₂ Z-scheme system for enhanced photocatalytic redox performance. *Appl. Surf. Sci.*, 2018. 448:288-296.
 226. Hu, M., Z. Xing, Y. Cao, Z. Li, X. Yan, Z. Xiu, T. Zhao, S. Yang, and W. Zhou, Ti³⁺ self-doped mesoporous black TiO₂/SiO₂/g-C₃N₄ sheets heterojunctions as remarkable visible-lightdriven photocatalysts. *Appl. Catal., B: Environ.*, 2018. 226:499-508.
 227. Lu, L., G. Wang, M. Zou, J. Wang, and J. Li, Effects of calcining temperature on formation of hierarchical TiO₂/g-C₃N₄ hybrids as an effective Z-scheme heterojunction photocatalyst. *Appl. Surf. Sci.*, 2018. 441:1012-1023.
 228. Zhong, R., Z. Zhang, H. Yi, L. Zeng, C. Tang, L. Huang, and M. Gu, Covalently bonded 2D/2D O-g-C₃N₄/TiO₂ heterojunction for enhanced visible-light photocatalytic hydrogen evolution. *Appl. Catal., B: Environ.*, 2018. 237:1130-1138.

229. Ali, K.A., A.Z. Abdullah, and A.R. Mohamed, Visible light responsive TiO₂ nanoparticles modified using Ce and La for photocatalytic reduction of CO₂: Effect of Ce dopant content. *Appl. Catal. A: Gen.*, 2017. 537:111-120.
230. Zhang, C., Y. Zhou, J. Bao, J. Fang, S. Zhao, Y. Zhang, X. Sheng, and W. Chen, Structure regulation of ZnS@g-C₃N₄/TiO₂ nanospheres for efficient photocatalytic H₂ production under visible-light irradiation. *Chem. Eng. J.*, 2018. 346:226-237.
231. Deng, F., L. Zhao, X. Luo, S. Luo, and D.D. Dionysiou, Highly efficient visible-light photocatalytic performance of Ag/AgIn₅S₈ for degradation of tetracycline hydrochloride and treatment of real pharmaceutical industry wastewater. *Chem. Eng. J.*, 2018. 333:423-433.
232. Hafeez, H.Y., S.K. Lakhera, S. Bellamkonda, G.R. Rao, M.V. Shankar, D.W. Bahnemann, and B. Neppolian, Construction of ternary hybrid layered reduced graphene oxide supported g-C₃N₄-TiO₂ nanocomposite and its photocatalytic hydrogen production activity. *Int. J. Hydrogen Energy*, 2018. 43(8):3892-3904.
233. Khalid, N.R., E. Ahmed, Z. Hong, and M. Ahmad, Synthesis and photocatalytic properties of visible light responsive La/TiO₂-graphene composites. *Appl. Surf. Sci.*, 2012. 263:254-259.
234. Guo, N., Y. Zeng, H. Li, X. Xu, H. Yu, and X. Han, Novel mesoporous TiO₂@g-C₃N₄ hollow core@shell heterojunction with enhanced photocatalytic activity for water treatment and H₂ production under simulated sunlight. *Journal of hazardous materials*, 2018. 353:80-88.
235. Wang, W., X. Liu, J. Fang, and C. Lu, TiO₂@g-C₃N₄ heterojunction with directional charge migration behavior for photodegradation of tetracycline antibiotics. *Mater. Lett.*, 2019. 236:622-624.
236. Nie, Y.-C., F. Yu, L.-C. Wang, Q.-J. Xing, X. Liu, Y. Pei, J.-P. Zou, W.-L. Dai, Y. Li, and S.L. Suib, Photocatalytic degradation of organic pollutants coupled with simultaneous photocatalytic H₂ evolution over graphene quantum dots/Mn-N-TiO₂/g-C₃N₄ composite catalysts: Performance and mechanism. *Appl. Catal., B: Environ.*, 2018. 227:312-321.
237. Gonell, F., A.V. Puga, B. Julián-López, H. García, and A. Corma, Copper-doped titania photocatalysts for simultaneous reduction of CO₂ and production of H₂ from aqueous sulfide. *Appl. Catal., B: Environ.*, 2016. 180:263-270.

238. Yu, Y., L. Piao, J. Xia, W. Wang, J. Geng, H. Chen, X. Xing, and H. Li, A facile one-pot synthesis of N-La codoped TiO₂ porous materials with bio-hierarchical architectures and enhanced photocatalytic activity. *Mater. Chem. Phys.*, 2016. 182:77-85.
239. Liu, Y., S. Zhou, J. Li, Y. Wang, G. Jiang, Z. Zhao, B. Liu, X. Gong, A. Duan, J. Liu, Y. Wei, and L. Zhang, Photocatalytic reduction of CO₂ with water vapor on surface La-modified TiO₂ nanoparticles with enhanced CH₄ selectivity. *Appl. Catal., B: Environ.*, 2015. 168-169:125-131.
240. Crake, A., K.C. Christoforidis, R. Godin, B. Moss, A. Kafizas, S. Zafeirotos, J.R. Durrant, and C. Petit, Titanium dioxide/carbon nitride nanosheet nanocomposites for gas phase CO₂ photoreduction under UV-visible irradiation. *Appl. Catal., B: Environ.*, 2019. 242:369-378.
241. Nie, N., L. Zhang, J. Fu, B. Cheng, and J. Yu, Self-assembled hierarchical direct Z-scheme g-C₃N₄/ZnO microspheres with enhanced photocatalytic CO₂ reduction performance. *Appl. Surf. Sci.*, 2018. 441:12-22.
242. Zheng, H., Z. Jiang, H. Zhai, Z. Zheng, P. Wang, Z. Wang, Y. Liu, X. Qin, X. Zhang, and B. Huang, Ag^{nt} quantum dots obtained via in situ photodeposition method as photocatalytic CO₂ reduction cocatalyst: Borrowing redox conversion between Ag⁺ and Ag⁰. *Appl. Catal., B: Environ.*, 2019. 243:381-385.
243. Li, H., Y. Gao, X. Wu, P.-H. Lee, and K. Shih, Fabrication of Heterostructured g-C₃N₄/Ag-TiO₂ Hybrid Photocatalyst with Enhanced Performance in Photocatalytic Conversion of CO₂ Under Simulated Sunlight Irradiation. *Appl. Surf. Sci.*, 2017. 402:198-207.
244. Li, K., T. Peng, Z. Ying, S. Song, and J. Zhang, Ag-loading on brookite TiO₂ quasi nanocubes with exposed {2 1 0} and {0 0 1} facets: Activity and selectivity of CO₂ photoreduction to CO/CH₄. *Appl. Catal., B: Environ.*, 2016. 180:130-138.
245. Li, H., Y. Gao, Z. Xiong, C. Liao, and K. Shih, Enhanced selective photocatalytic reduction of CO₂ to CH₄ over plasmonic Au modified g-C₃N₄ photocatalyst under UV-vis light irradiation. *Appl. Surf. Sci.*, 2018. 439:552-559.

246. Tahir, B., M. Tahir, and N.S. Amin, Performance analysis of monolith photoreactor for CO₂ reduction with H₂. *Energy Convers. Manage.*, 2015. 90:272-281.
247. Shi, D., Y. Feng, and S. Zhong, Photocatalytic conversion of CH₄ and CO₂ to oxygenated compounds over Cu/CdS–TiO₂/SiO₂ catalyst. *Catal. Today*, 2004. 98(4):505-509.
248. Liu, Z., G. Lu, Y. Guo, Y. Wang, and Y. Guo, Catalytic performance of La_{1-x}Er_xCoO₃ perovskite for the deoxidization of coal bed methane and role of erbium in a catalyst. *Catal. Sci. Technol.*, 2011. 1(6):1006.
249. Khalilzadeh, A. and A. Shariati, Photoreduction of CO₂ over heterogeneous modified TiO₂ nanoparticles under visible light irradiation: Synthesis, process and kinetic study. *Solar Energy*, 2018. 164:251-261.